Cell Reports

Article

SIRT6 transcriptionally regulates fatty acid transport by suppressing PPARγ

Graphical abstract

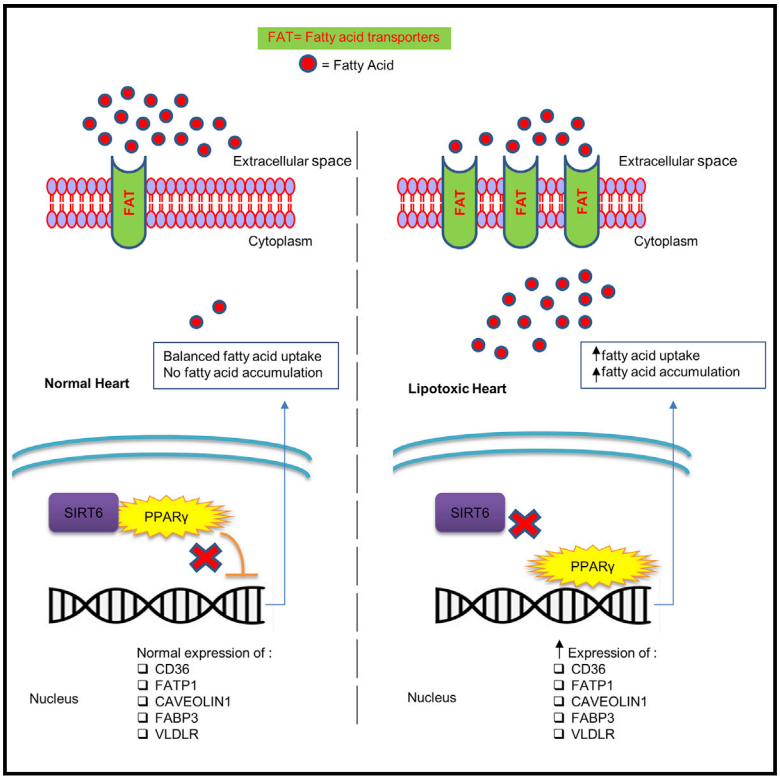

Highlights

- SIRT6 deficiency increases fatty acid uptake and lipid accumulation in cardiomyocytes
- SIRT6 deficiency transcriptionally upregulates the fatty acid transporter genes
- SIRT6 controls fatty acid transporter genes through the PPARγ transcription factor
- SIRT6 binds to the DNA-binding domain of PPARγ to regulate its activity

Authors

Danish Khan, Tarannum Ara, Venkatraman Ravi, ..., Prasanna Simha Mohan Rao, Narayanaswamy Srinivasan, Nagalingam Ravi Sundaresan

Correspondence

rsundaresan@iisc.ac.in

In brief

Khan et al. show that SIRT6, a nuclear sirtuin, regulates the transcription of fatty acid transporter genes in the heart through the PPARγ transcription factor in a deacetylase-independent manner. Notably, deficiency of SIRT6 causes increased fatty acid uptake and lipid accumulation in the heart.

Khan et al., 2021, Cell Reports *35*, 109190
June 1, 2021
https://doi.org/10.1016/j.celrep.2021.109190

CellPress

Cell Reports

CellPress
OPEN ACCESS

Article

SIRT6 transcriptionally regulates fatty acid transport by suppressing PPARγ

Danish Khan,[1] Tarannum Ara,[1] Venkatraman Ravi,[1] Raksha Rajagopal,[1] Himani Tandon,[2] Jayadevan Parvathy,[2,3] Edward A. Gonzalez,[4] Ninitha Asirvatham-Jeyaraj,[1] Swati Krishna,[1] Sneha Mishra,[1] Sukanya Raghu,[1] Arvind Singh Bhati,[1] Ankit Kumar Tamta,[1] Subhajit Dasgupta,[1] Ullas Kolthur-Seetharam,[5,6] Jean-Pierre Etchegaray,[4] Raul Mostoslavsky,[7] Prasanna Simha Mohan Rao,[8] Narayanaswamy Srinivasan,[2] and Nagalingam Ravi Sundaresan[1,9,*]

[1]Cardiovascular and Muscle Research Laboratory, Department of Microbiology and Cell Biology, Indian Institute of Science, Bengaluru, India
[2]Molecular Biophysics Unit, Indian Institute of Science, Bengaluru, India
[3]IISc-Mathematics Initiative, Indian Institute of Science, Bengaluru, India
[4]Department of Biological Sciences, Rutgers University, Newark, NJ, USA
[5]Tata Institute of Fundamental Research, Colaba, Mumbai, India
[6]Tata Institute of Fundamental Research, Hyderabad, India
[7]The Massachusetts General Hospital Cancer Center, Harvard Medical School, Boston, MA, USA
[8]Sri Jayadeva Institute of Cardiovascular Sciences and Research, Bengaluru, India
[9]Lead contact
*Correspondence: rsundaresan@iisc.ac.in
https://doi.org/10.1016/j.celrep.2021.109190

SUMMARY

Pathological lipid accumulation is often associated with enhanced uptake of free fatty acids via specific transporters in cardiomyocytes. Here, we identify SIRT6 as a critical transcriptional regulator of fatty acid transporters in cardiomyocytes. We find that SIRT6 deficiency enhances the expression of fatty acid transporters, leading to enhanced fatty acid uptake and lipid accumulation. Interestingly, the haploinsufficiency of SIRT6 is sufficient to induce the expression of fatty acid transporters and cause lipid accumulation in murine hearts. Mechanistically, SIRT6 depletion enhances the occupancy of the transcription factor PPARγ on the promoters of critical fatty acid transporters without modulating the acetylation of histone 3 at Lys 9 and Lys 56. Notably, the binding of SIRT6 to the DNA-binding domain of PPARγ is critical for regulating the expression of fatty acid transporters in cardiomyocytes. Our data suggest exploiting SIRT6 as a potential therapeutic target for protecting the heart from metabolic diseases.

INTRODUCTION

The heart is a highly dynamic organ that gets >70% of its ATP demands through the oxidation of fatty acids (Bertero and Maack, 2018). The process of fatty acid uptake and its oxidation is tightly coupled, which leaves only a tiny amount of fat stored as neutral lipids in the heart (Schulze et al., 2016). When the fatty acid uptake exceeds its oxidation rate, lipid accumulation occurs in the cardiomyocytes (Drosatos and Schulze, 2013). The excess accumulation of lipids triggers apoptosis, mitochondrial dysfunction, unfolded protein response, and inflammation in the heart (Bertero and Maack, 2018). Previous studies implicate fatty acid transporters as playing a significant role in the pathogenesis of cardiac diseases (Chabowski et al., 2008; Glatz et al., 2013). Interestingly, the fatty acid transporters are regulated by transcriptional and post-transcriptional mechanisms (Bonen et al., 2002). However, the molecular players involved in their regulation are not entirely understood.

Sirtuins are a class of nicotinamide adenine dinucleotide-positive (NAD^+)-dependent enzymes that act as nutrient sensors and play a vital role in regulating cellular metabolism (Feldman et al., 2012). Notably, sirtuins mediate the benefits of calorie restriction (Houtkooper et al., 2012). Seven sirtuin isoforms (SIRT1–7) localize to different subcellular compartments and control a broad range of biological processes, including metabolism, gene expression, DNA repair, and inflammation (Houtkooper et al., 2012). Of these, the nuclear-localized SIRT6 deacetylates histone 3 at Lys 9 and Lys 56 to control the transcription of a wide range of genes linked to metabolism, inflammation, and DNA repair (Kugel and Mostoslavsky, 2014). Specifically, SIRT6 plays a crucial role in regulating glucose and lipid metabolism (Kim et al., 2010; Zhong et al., 2010). We have previously shown that SIRT6 promotes mitochondrial oxidation in the heart (Khan et al., 2018). Further, SIRT6 regulates cholesterol biosynthesis and fatty acid metabolism, especially fatty acid oxidation in the liver (Elhanati et al., 2013; Naiman et al., 2019). Despite its essential roles in lipid homeostasis, its precise role in regulating fatty acid uptake in the heart is unclear.

Fatty acids are transported into the cardiomyocytes either through passive uptake or through specific transporters such as fatty acid transport (FAT)/CD36, FAT protein 1 (FATP1) and caveolin-1. Fatty acid-binding protein 3 (FABP3) plays an essential role in intracellular fatty acid transport (Bonen et al., 2002). Notably, the elevated expression of these transporters leads to

the accumulation of lipid in the heart, thereby inducing cardiac dysfunction through lipotoxicity (Chiu et al., 2005; Glatz et al., 2013; Perman et al., 2011). Previous studies indicate that the fatty acid transporters are transcriptionally regulated by peroxisome proliferator-activated receptors (PPARs) (Glatz et al., 2010; Motojima et al., 1998). There are three PPAR isoforms—PPARα, PPARγ, and PPARδ—and they function as a heterodimer with the retinoid X receptor (RXR) (Lee and Kim, 2015). They regulate different aspects of lipid metabolism and energy balance in the heart, skeletal muscle, liver, and adipose tissue (Braissant et al., 1996). While PPARα and PPARβ/δ mainly facilitate energy combustion and play a crucial role in fatty acid oxidation, PPARγ contributes to energy storage by enhancing adipogenesis (Auwerx, 1999; Rao et al., 2002). Notably, cardiac-specific overexpression of PPARγ induces lipotoxicity in the heart (Son et al., 2007). However, the exact mechanisms of how PPARγ is regulated in the heart is not well understood.

In the present study, we describe an essential role for SIRT6 in regulating fatty acid uptake in cardiomyocytes through the transcriptional regulation of the fatty acid transporters via the PPARγ transcription factor.

RESULTS

The levels of SIRT6 were reduced in mice models of diabetic cardiomyopathy

Previously, we found that cardiac SIRT6 levels reduced in patients with heart failure (Sundaresan et al., 2012). Since lipotoxicity is one of the significant contributors to heart failure in patients with metabolic disease (Drosatos and Schulze, 2013), we analyzed the levels of SIRT6 in the hearts of diabetic mice. In line with previous reports, mice harboring a mutation in the leptin receptor (*db/db*) had significantly higher blood glucose levels (Figure 1A) (Coleman and Hummel, 1967) and higher fat deposition in the heart (Figure 1B). While the expression of fatty acid transporters CD36, FATP1, and very-low-density lipoprotein receptor (VLDLR) was upregulated (Figure 1C), the levels of SIRT6 were significantly low in the hearts of *db/db* mice (Figures 1D and S1A). We next tested a high-fat diet (HFD)-fed diabetic mouse model to verify these findings and found similar results (Figures S1B and S1C). Therefore, these results indicate an inverse correlation between SIRT6 and fatty acid transporters in diabetic mouse hearts.

SIRT6 negatively regulates fatty acid uptake in cardiomyocytes

To evaluate the effect of SIRT6 on fatty acid uptake, we transiently depleted SIRT6 in primary cardiomyocytes and followed the uptake of BODIPY-labeled fatty acids using confocal microscopy. Interestingly, we found that the uptake of fatty acids increased in SIRT6-knockdown (KD) cardiomyocytes (Figures 1E and S1D). We further analyzed the number of lipid droplets and their size in our confocal images. We found an appreciable increase in the number and average size of lipid droplets in the cardiomyocytes upon SIRT6 depletion (Figures S1E and S1F). Similarly, flow cytometry-based fatty acid uptake assay revealed a significant increase in fatty acid uptake in SIRT6KD cardiomyocytes (Figure 1F). Also, we observed higher fatty acid uptake in SIRT6 knockout (KO) murine embryonic fibroblasts (MEFs), and SIRT6-depleted HeLa cells (Figures S1G and S1H). Conversely, fatty acid uptake significantly reduced in SIRT6-overexpressed cardiomyocytes. Further analysis suggested that SIRT6 overexpression significantly reduced the total number of droplets and their average size (Figures S1I–S1M)

Surprisingly, the catalytically inactive mutants of SIRT6 effectively suppressed fatty acid uptake similar to wild-type (WT) SIRT6 (Figures 1G,1H, S1N, and S1O). Moreover, the reconstitution of either WT or mutant SIRT6 reduced fatty acid uptake in SIRT6-depleted cardiomyocytes (Figures 1I and S1P). These findings suggest that SIRT6 regulates fatty acid uptake independent of its catalytic activity. Next, we tested whether SIRT6 modulates lipid accumulation in cardiomyocytes using the lipid-binding dye BODIPY. Consistently, SIRT6 depletion significantly increased the lipid accumulation, while its overexpression suppressed lipid accumulation in cardiomyocytes (Figures 1J–1L). Notably, oil red O staining of cardiac tissues of SIRT6 heterozygous mice revealed increased fatty acid accumulation, suggesting that reducing SIRT6 levels increases lipid accumulation in the heart (Figure 1M). Overall, these results suggest that SIRT6 deficiency increases fatty acid uptake and lipid accumulation in the cardiomyocytes.

SIRT6 negatively regulates the expression of fatty acid transporters

Studies indicate that the uptake of fatty acids is regulated by specific transporters in cardiomyocytes (van der Vusse et al., 2000). Therefore, we tested the expression of these fatty acid transporters in SIRT6KO and SIRT6 heterozygous mice hearts. Interestingly, we observed a significant increase in the expression of CD36 and caveolin-1 in SIRT6KO mice hearts. Moreover, we observed the increased expression of FABP3, which binds fatty acids in the cytosol and transports it to the nucleus, leading to the activation of lipid-activated transcription factors such as PPARγ (Shan et al., 2009). The expression of PPARγ, a key regulator of fatty acid transporters, also increased (Figures 2A and S2A) (Auwerx, 1999). These results suggest that SIRT6 deficiency leads to the increased expression of fatty acid transporters and PPARγ in the heart. We observed that except for CD36 in the lung, the expression of other fatty acid transporter genes was upregulated in the kidney, muscle, and lung of SIRT6KO mice (Figures 2B, 2C, and S2B–S2E), suggesting a conserved mechanism of regulation across different tissues of mice. Along similar lines, we found that the expression of CD36, caveolin-1, FABP3, and PPARγ increased significantly, even under conditions of SIRT6 haploinsufficiency (Figures 2D and S2F). Next, we tested whether SIRT6 regulates the expression of fatty acid transporters in a cell-autonomous manner in cardiomyocytes. Our immunofluorescence analysis revealed that the levels of CD36, caveolin-1, VLDLR, and FABP3 increased upon SIRT6 depletion. Similarly, the expression of fatty acid transporters reduced in SIRT6-overexpressed cardiomyocytes, in agreement with our *in vivo* results (Figures 2E and S2G–S2J). Also, our immunoblotting analysis revealed that the expression of caveolin-1, as well as CD36, reduced markedly in cardiomyocytes transfected with either WT or catalytic mutants of SIRT6 (Figures 2F and 2G), which is consistent with our observations on the enzymatic activity-independent effect of SIRT6 on fatty acid uptake. Collectively, these results indicate

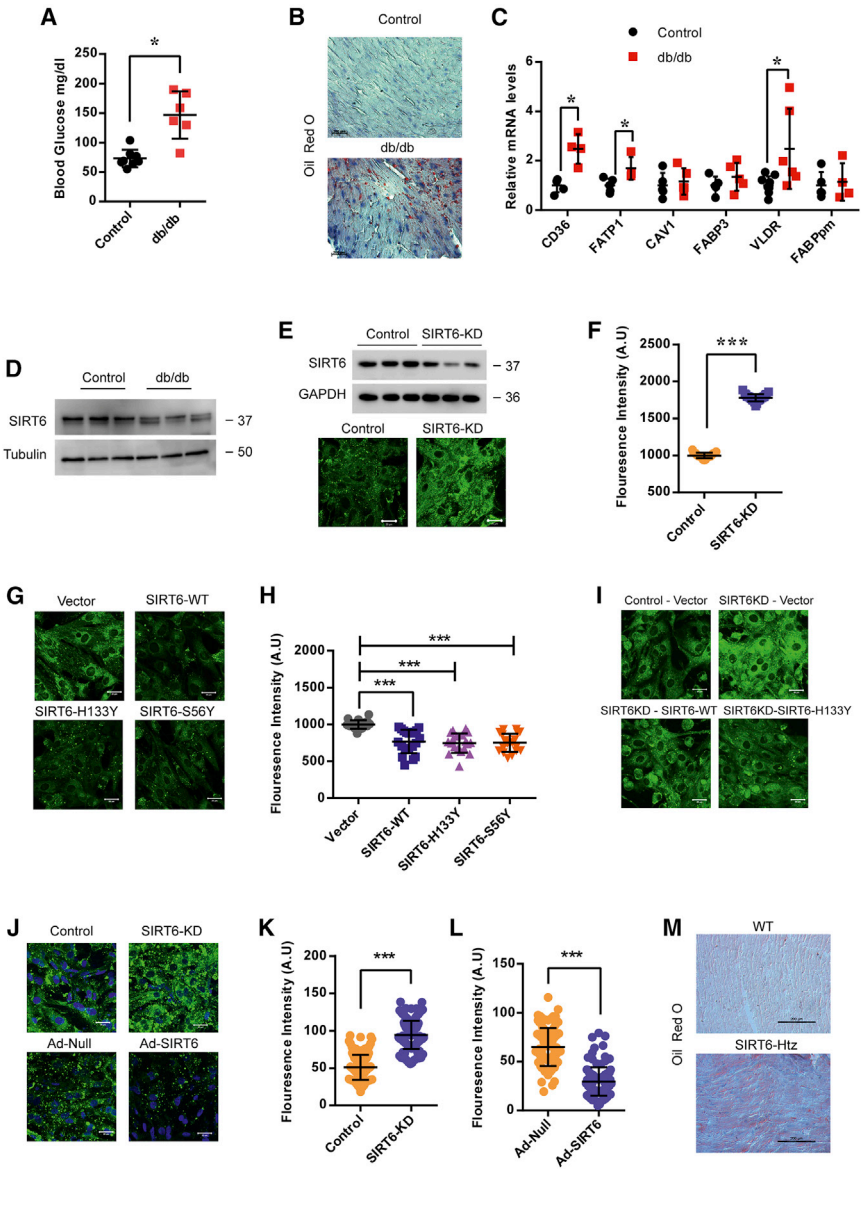

Figure 1. SIRT6 is a critical regulator of fatty acid uptake

(A) Fasting blood glucose levels in control and *db/db* mice. n = 6–8 mice per group, Student's t test, data presented as means ± SDs, *p < 0.05.

(B) Lipid accumulation in the heart section of control and *db/db* mice assessed by oil red O staining. Scale bar, 200 μm, n = 5 mice per group.

(C) The mRNA levels of indicated fatty acid transporters in the heart of wild-type (WT) and *db/db* mice, n = 4–9 mice per group, Student's t test, data presented as means ± SDs, *p < 0.05.

(D) Western blot images showing the levels of SIRT6 in WT and *db/db* mice, n = 3 mice per group.

(E) Fatty acid uptake in SIRT6-depleted primary cardiomyocytes. Cells were treated with BODIPY-labeled fatty acid (green) for 30 min, n = 3 independent experiments, scale bar, 20 μm (lower panel). SIRT6 depletion was confirmed by western blotting (upper panel).

(F) The fatty acid uptake in SIRT6-depleted primary cardiomyocytes measured by flow cytometry, n = 23 samples per group, data presented as means ± SDs Student's t test, ***p < 0.0005.

(G) Uptake of BODIPY-labeled fatty acids (green) in primary cardiomyocytes transfected with either vector, SIRT6-WT, SIRT6-H133Y, or SIRT6-S56Y plasmids for 60 h, n = 3 independent experiments, scale bar, 20 μm.

(H) Flow cytometry-based measurement of fatty acid uptake in primary cardiomyocytes transfected with either vector, SIRT6-WT, SIRT6-H133Y, or SIRT6-S56Y plasmids, n = 17–20, data presented as means ± SDs, 1-way ANOVA, ***p < 0.0005.

(I) Fatty acid uptake in SIRT6-depleted primary cardiomyocytes transfected with vector, SIRT6-WT, or SIRT6-H133Y, scale bar, 20 μm.

(J) Representative confocal images depicting lipid accumulation in SIRT6-depleted and SIRT6-overexpressed primary cardiomyocytes. Lipids were stained with the dye BODIPY (green). The nucleus was stained with Hoechst 33342. n = 3 independent experiments, scale bar, 20 μm.

(K and L) Quantification of lipid accumulation in SIRT6-depleted cardiomyocytes (K), and SIRT6-overexpressed cardiomyocytes (L), n = 99–158 cells per group, Student's t test, data presented as means ± SDs, ***p < 0.0005.

(M) Lipid accumulation in heart sections of WT and SIRT6$^{+/-}$ mice stained with oil red O, scale bar, 200 μm, n = 5 mice per group.

that SIRT6 controls the expression of fatty acid transporters in the cardiomyocytes independent of its catalytic activity in a cell-autonomous manner.

SIRT6 transcriptionally regulates the expression of fatty acid transporters

SIRT6 is a chromatin-associated protein known to regulate the expression of several genes (Kugel and Mostoslavsky, 2014). Therefore, we analyzed the expression of fatty acid transporters in our previously generated RNA sequencing (RNA-seq) dataset from WT and SIRT6KO embryonic stem cells (ESCs) (Etchegaray et al., 2019). Interestingly, we found that the levels of fatty acid transporters such as CD36, caveolin-1, FATP1, and FABP3 were upregulated in SIRT6KO ESCs (Figure 3A). However, the expression of the cholesterol transporter VLDLR downregulated in SIRT6KO ESCs (Figure 3A). To confirm whether these changes are relevant to the heart, we performed a qPCR analysis of fatty acid transporter genes. Our results revealed that the mRNA levels of multiple fatty acid transporters increased in SIRT6KO and heterozygous mice hearts. Further, the levels of cholesterol transporter VLDLR upregulated in SIRT6KO mice hearts (Figures 3B and 3C). Conversely, the expression of these transporters was reduced in SIRT6-overexpressing cardiomyocytes (Figure 3D). Notably, overexpression of catalytically inactive

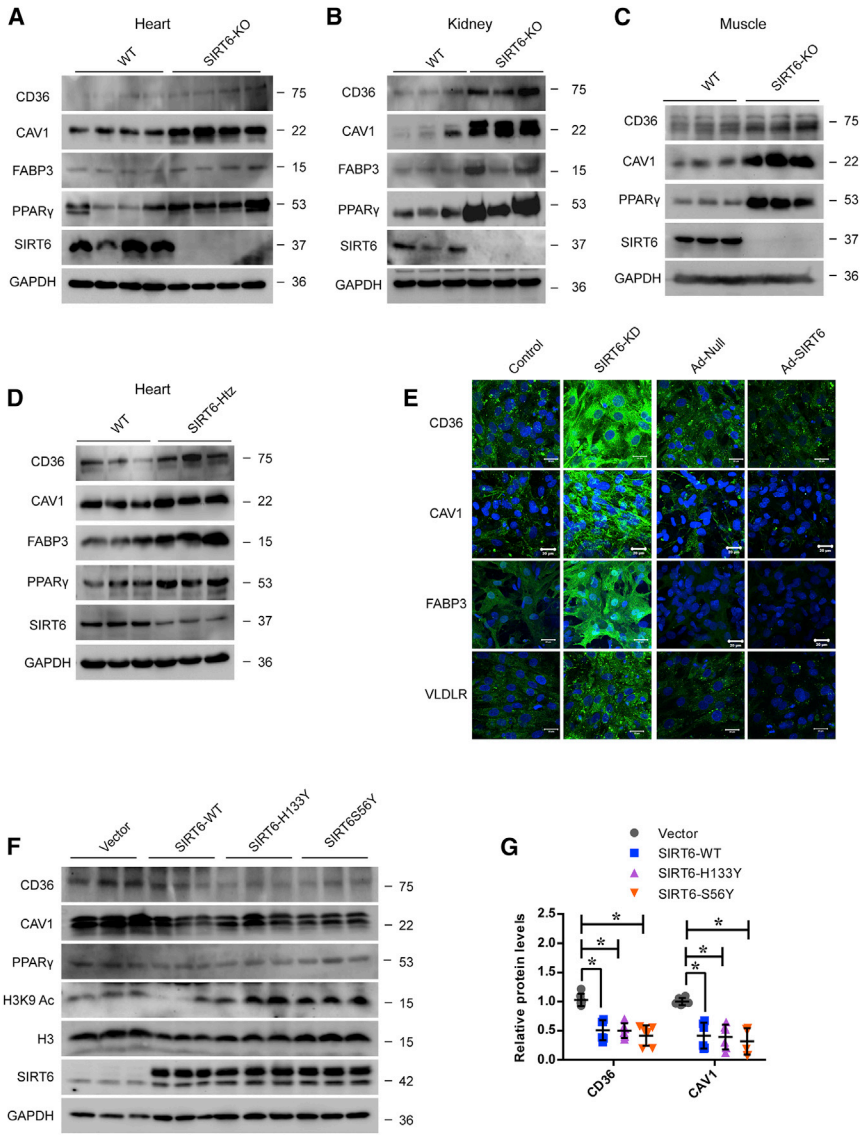

Figure 2. SIRT6 deficiency upregulates fatty acid transporters

(A) The levels of fatty acid transporters in the hearts of SIRT6 knockout (SIRT6KO) mice measured by western blotting, n = 4 mice per group.

(B and C) Fatty acid transporters expression in the kidney (B) and muscle (C) of SIRT6KO mice, n = 3 mice per group.

(D) The levels of fatty acid transporters in the hearts of SIRT6 heterozygous mice, n = 3 mice per group.

(E) Representative confocal images showing the level of fatty acid transporters (stained green) in SIRT6-depleted and SIRT6-overexpressing primary cardiomyocytes. n = 3 independent experiments, scale bar, 20 μm. SIRT6 depletion and overexpression were confirmed by immunoblotting, as shown in Figures S2G and S2H.

(F) The levels of fatty acid transporters in the primary cardiomyocytes transfected with either vector, SIRT6-WT, SIRT6-H133Y, or SIRT6-S56Y plasmids. n = 6.

(G) Quantification of fatty acid transporter protein levels in the primary cardiomyocytes transfected with either vector, SIRT6-WT, SIRT6-H133Y, or SIRT6-S56Y plasmids. Data presented as means ± SDs, n = 6, 1-way ANOVA, *p < 0.05.

SIRT6-H133Y also downregulated the expression of fatty acid transporters, except for FATP1 (Figure 3D). Further, we found that reconstitution of both WT and mutant SIRT6 could significantly reduce the expression of CD36, CAV1, and VLDR in SIRT6-depleted cardiomyocytes (Figure 3E). Our results show that the protein levels of fatty acid transporters were reduced in SIRT6KD cells when WT or catalytically inactive mutants of SIRT6 were overexpressed (Figure S3A). These findings reveal that SIRT6 regulates the expression of fatty acid transporters independent of its catalytic activity.

Since we observed that SIRT6 depletion increases lipid accumulation, we next tested the expression of genes involved in the fatty acid synthesis and oxidation pathways. Notably, the mRNA levels of major genes involved in fatty acid biosynthesis, such as FAS and SCD1, were significantly upregulated in the hearts of SIRT6-deficient mice (Figure S3B). However, we did not observe any marked changes in the expression of genes involved in fatty acid oxidation, except CPT1 (Figure S3C). Similarly, we did not observe any significant changes in the mRNA levels of key enzymes in the tricarboxylic acid (TCA) cycle except for succinate dehydrogenase (SDH), which was downregulated (Figure S3D). Since fatty acid uptake plays a crucial role in lipid accumulation (van der Vusse et al., 2000), we focused further on fatty acid uptake genes. We analyzed the binding of SIRT6 on the promoters of fatty acid transporters, taking advantage of the previous SIRT6 chromatin immunoprecipitation sequencing ChIP-seq dataset in mouse ESCs (Etchegaray et al., 2019). Our analysis in WT and SIRT6KO ESCs indicated that SIRT6 binds to the promoters of fatty acid transporter genes (Figure 3F). Interestingly, we found that SIRT6 is also localized at promoter-proximal pausing sites downstream of the transcription start site (Etchegaray et al., 2019). We next analyzed the previously reported ChIP-seq dataset from K562 cells and H1 cells (Dunham et al., 2012) and observed the binding of SIRT6 to the promoters of fatty acid transporter genes in K562 cells and H1 cells (Figure S3E). Our ChIP-qPCR analysis confirmed that SIRT6 binds to the promoters of the fatty acid transporter genes in the heart (Figure 3G), indicating a possible contribution of SIRT6 in regulating their expression.

SIRT6 controls fatty acid uptake through the PPARγ transcription factor

Previous studies indicate that the expression of fatty acid transporters is regulated by the PPAR family of transcription factors

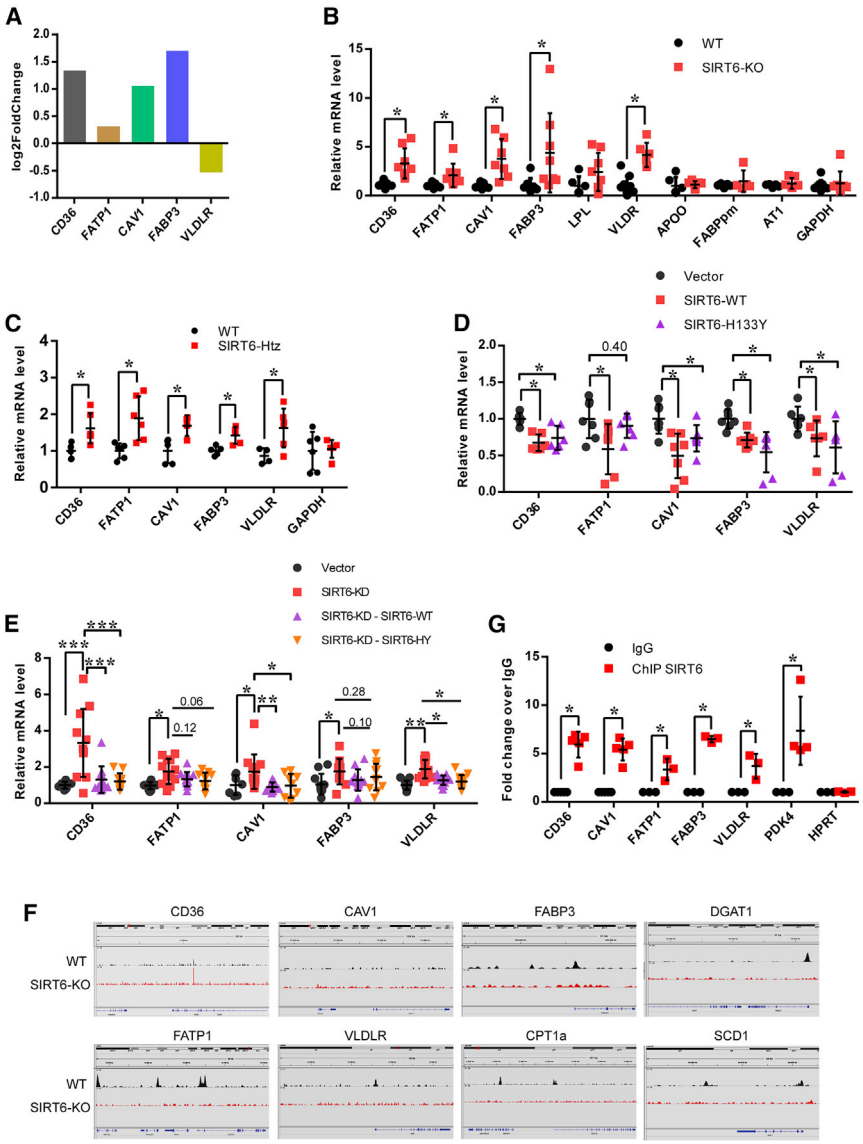

Figure 3. SIRT6 transcriptionally regulates the fatty acid transporters

(A) RNA-seq analysis of the WT and SIRT6KO ESCs revealing relative mRNA levels of indicated genes in log scale (GEO: GSE130690).

(B) The mRNA levels of genes involved in fatty acid and lipid uptake in the heart of WT and SIRT6 knockout mice. Data presented as means ± SDs, n = 5–10 mice per group, Student's t test, *p < 0.05. Glyceraldehyde 3-phosphate dehydrogenase (GAPDH) and AT1, negative controls.

(C) The mRNA levels of fatty acid transporters in the hearts of WT and SIRT6 heterozygous mice. Data presented as means ± SDs, n = 4–6 mice per group, Student's t test, *p < 0.05.

(D) The mRNA levels of fatty acid transporters in the control, SIRT6-WT, and SIRT6-H133Y mutant-overexpressing cardiomyocytes. Data presented as means ± SDs, n = 6–7, 1-way ANOVA, *p < 0.05.

(E) The mRNA levels of fatty acid transporters in SIRT6-depleted cardiomyocytes reconstituted with SIRT6-WT or SIRT6-H133Y mutant. Data presented as means ± SDs, n = 7–13 per group, 2-way ANOVA, *p < 0.05,**p < 0.005,***p < 0.0005.

(F) ChIP-seq data showing occupancy of SIRT6 in the genomic regions surrounding the transcription start site of indicated genes in WT and SIRT6 knockout human ESCs (hESCs) (GEO: GSE130689).

(G) ChIP analysis showing SIRT6 binding on the promoters of indicated fatty acid transporters in the heart. n = 3–5 mice per group. Data are presented as means ± SDs, Student's t test, *p < 0.05. Pyruvate dehydrogenase kinase 4 (PDK4), positive control; hypoxanthine phosphoribosyl transferase (HPRT), negative control.

(Lee and Kim, 2015). A recent study reported that SIRT6 activates the PPARα transcription factor, which regulates genes involved in fatty acid oxidation in the liver (Naiman et al., 2019). We, therefore, focused on PPARγ, a significant regulator of fatty acid transporters (Schaiff et al., 2005); Son et al., 2007). Our immunoblotting analysis revealed that the levels of PPARγ upregulated in SIRT6KO mice hearts (Figure S4A). However, we did not observe any marked changes in the mRNA levels of Pparg (Figure S4B), which has been shown to undergo alternate splicing and code for multiple isoforms (Aprile et al., 2018). Specifically, the Pparg2 variant mRNA in the mouse contains an additional exon before the exon1 of Pparg1. We checked the level Pparg2 using specific primers for this exon, but we did not find any significant change in its expression between WT and SIRT6KO mice hearts (Figure S4B). Also, we did not find any changes in the Pparg isoform with exon 5 deletion (Figures S4C and S4D), which results in the loss of the ligand-binding domain (Aprile et al., 2018). Since we did not see any significant differences in any of the Pparg isoforms tested, we believe that Pparg could be regulated at the post-transcriptional level.

Since SIRT6 regulates the levels of PPARγ, we hypothesized that SIRT6 could modulate fatty acid uptake through PPARγ. To test this, we treated cells with GW9662, an irreversible PPARγ antagonist, to see whether the inhibition of PPARγ could rescue the increased fatty acid uptake observed under SIRT6-depleted conditions. Analysis of fatty acid uptake by confocal microscopy revealed that treatment with GW9662 abrogated the increased fatty acid uptake in SIRT6-depleted cardiomyocytes (Figures 4A and S4E). Similarly, we observed that GW9662 treatment abrogated the increased lipid accumulation in SIRT6-depleted cardiomyocytes (Figures 4B and S4F). Furthermore, GW9662 treatment attenuated the increase in the expression of fatty acid transporters in SIRT6-depleted cells (Figure 4C). Consistently, our qPCR analysis revealed that treatment with PPARγ antagonist significantly reduced the increased levels of CD36, CAV1, and FABP3 in SIRT6-depleted cardiomyocytes but not that of FATP1 or VLDLR, suggesting that there may be additional factors involved in the regulation of FATP1 and VLDLR under SIRT6-depleted conditions (Figure 4D).

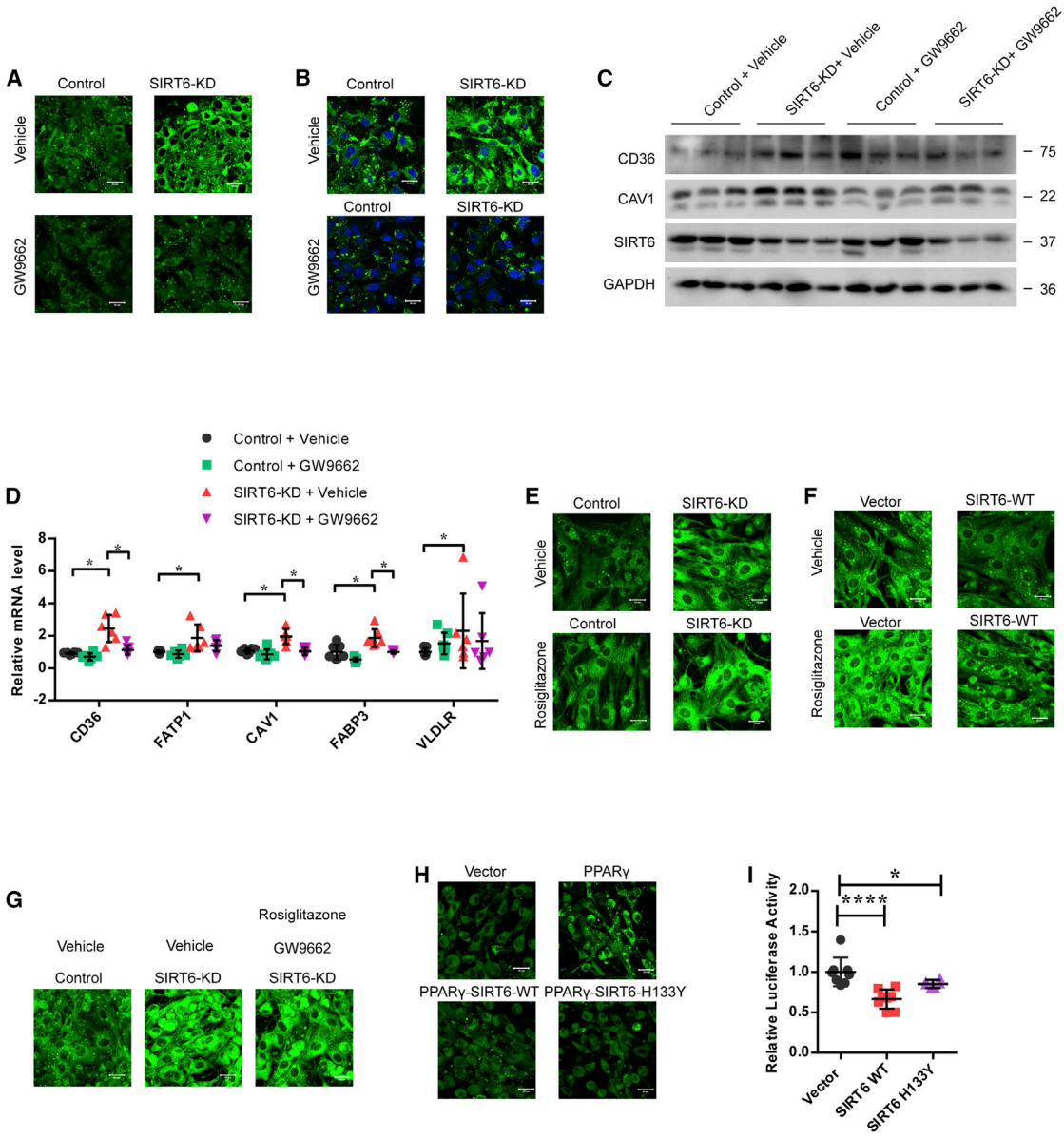

Figure 4. SIRT6 represses the transcription factor PPARγ

(A) Representative confocal images showing BODIPY-labeled fatty acids (green) in SIRT6-depleted cardiomyocytes treated with vehicle (DMSO) or PPARγ-specific irreversible PPARγ antagonist, GW9662 (5 μM). n = 4 independent experiments, scale bar, 20 μm.

(B) Confocal images showing lipid accumulation, as stained by BODIPY (green) in SIRT6-depleted cardiomyocytes treated with vehicle (DMSO) or PPARγ-specific irreversible PPARγ antagonist (5 μM), GW9662. Nuclei were stained with Hoechst 33342. Scale bar, 20 μm, n = 2 independent experiments.

(C) The levels of indicated fatty acid transporters in SIRT6-depleted cardiomyocytes treated with vehicle (DMSO) or GW9662, n = 3 per group (5 μM).

(D) The mRNA levels of fatty acid transporters in SIRT6-depleted cardiomyocytes treated with DMSO or GW9662. Data presented as means ± SDs, n = 6–7 per group, 2-way ANOVA, *p < 0.05 (5 μM).

(E) Representative confocal images showing BODIPY-labeled fatty acids (green) in SIRT6-depleted cardiomyocytes treated with vehicle (DMSO) or PPARγ-specific activator, rosiglitazone (50 μM). n = 3 independent experiments, scale bar, 20 μm.

(F) Representative confocal images showing BODIPY-labeled fatty acids (green) in SIRT6-overexpressing cardiomyocytes treated with vehicle (DMSO) or PPARγ-specific activator, rosiglitazone (50 μM). n = 3 independent experiments, scale bar, 20 μm.

(G) Representative confocal images showing BODIPY-labeled fatty acids (green) in SIRT6-depleted cardiomyocytes treated with vehicle (DMSO) or GW9662 (5 μM), followed by stimulation with rosiglitazone. The inhibitor and rosiglitazone were treated for 36 h (50 μM), followed by a fatty acid uptake experiment. n = 3 independent experiments, scale bar, 20 μm.

(H) Confocal microscopy analysis showing uptake of BODIPY-labeled fatty acid (green) in cells transfected with indicated plasmids. Scale bar, 20 μm, n = 2 independent experiments.

(I) The relative luciferase activity in HEK293T cells overexpressing PPARγ along with SIRT6-WT or SIRT6-H133Y. Renilla luciferase was used for normalization. Data presented as means ± SDs, n = 6–8 per group, 1-way ANOVA, *p < 0.05, ****p < 0.0005.

Furthermore, we observed that treatment with the PPARγ agonist rosiglitazone enhanced the increased fatty acid uptake observed in SIRT6-depleted cells (Figures 4E and S4G). Notably, the overexpression of SIRT6 attenuated the rosiglitazone-induced increase in fatty acid uptake (Figures 4F and S4H). Also, we observed that GW9662 pre-treatment abrogated the rosiglitazone-induced increase in fatty acid uptake in SIRT6-depleted cells (Figures 4G and S4I), indicating that PPARγ protein activation is essential for the SIRT6-mediated increase in fatty acid uptake. Since SIRT6 regulates fatty acid uptake independent of catalytic activity, we tested the effect of the WT or catalytic mutant of SIRT6 on PPARγ-induced fatty acid uptake. We found that PPARγ overexpression increased the fatty acid uptake in cardiomyocytes. However, the overexpression of either the WT or catalytic mutant of SIRT6 attenuated the increase in fatty acid uptake in these cells (Figures 4H and S4J). Moreover, our results suggest that SIRT6 suppresses CD36 promoter activity irrespective of its catalytic activity (Figure 4I). These data suggest that SIRT6 regulates fatty acid uptake in a catalytically independent manner through its action on PPARγ.

SIRT6 regulates PPARγ activity at the promoters by binding to its DNA-binding domain, the PPARγ transcription factor

To understand how SIRT6 could regulate PPARγ, we first tested the interaction between the two proteins. Our immunoprecipitation assays indicate that SIRT6 interacts with PPARγ (Figures 5A and 5B). SIRT6 can recruit acetyltransferases to alter the acetylation status of its binding partners (Dominy et al., 2012). However, we could not observe any detectible acetylation in PPARγ, even though histone H3, the positive control, was found to be acetylated (Figures S5A and S5B). We next tested whether the catalytic mutants of SIRT6 could interact with PPARγ similar to WT SIRT6 since we found that both WT and catalytic mutants of SIRT6 could regulate PPARγ target genes (Figures 2F, 3D, and 3E). Our immunoprecipitation analysis revealed that two different catalytic mutants of SIRT6 (H133Y and S56Y) could efficiently bind to PPARγ, similar to the WT SIRT6 (Figure 5C). Next, we were interested to see whether these proteins were closely associated with chromatin. Interestingly, PPARγ binding elements (PPRE) overlap with the region bound by SIRT6 in the promoters of CD36 and caveolin1 (Table S1). To experimentally verify whether both proteins bind to the same region, we performed ChIP for SIRT6 in the hearts of WT mice. We further used the chromatin pulled down with SIRT6 to perform re-ChIP for PPARγ. Our ChIP-re-ChIP experiments suggest that PPARγ is significantly enriched on the promoters of fatty acid transporters in the SIRT6 pull-down fraction (Figure 5D), indicating a close association between the two proteins in the chromatin context.

Previous studies have shown that SIRT6 could control the activity of transcription factors by regulating their occupancy at the promoters of their target genes (Sebastián et al., 2012; Sundaresan et al., 2012). Our ChIP analysis revealed that the occupancy of PPARγ at the promoters of CD36, caveolin-1, FATP1, FABP3, and VLDLR was significantly increased in SIRT6 heterozygous mice hearts (Figure 5E). We next tested whether SIRT6 haploinsufficiency alters the acetylation of histone 3 at Lys 9 (H3K9) at the promoters of fatty acid transporter genes. Although we observed an increase in the global H3K9 acetylation levels in SIRT6 heterozygous mice, we did not observe any marked changes in H3K9 acetylation at the promoters of fatty acid transporter genes. (Figures 5F and S5C). Similar to H3K9, we did not detect any marked difference in the acetylation status of H3K56 at the promoter region of fatty acid transporters (Figure 5G). These results suggest that SIRT6 regulates PPARγ occupancy at the promoters of fatty acid transporters genes independent of H3K9 and H3K56 acetylation, which is consistent with the enzymatic activity-independent regulation of fatty acid uptake by SIRT6.

Our recent study noted that both the WT and the catalytic mutants of SIRT6 could regulate the occupancy of the Sp1 transcription factor by binding to its zinc-finger DNA-binding domain (Ravi et al., 2019). We therefore hypothesized that SIRT6 could similarly regulate PPARγ activity by binding to its DNA-binding domain. To predict the binding mode of SIRT6 with PPARγ, we performed an *in silico* molecular docking analysis using the structures available in the Protein Data Bank (PDB) (Pan et al., 2011; Chandra et al., 2008; Berman et al., 2000). Rather than performing blind docking with SIRT6 and PPARγ, we predicted the likely interface residues on both of the structures and used them as restraints while docking using HADDOCK and HDOCK (van Zundert et al., 2016; Yan et al., 2017). Interfacial residues were predicted by analyzing the multiple sequence alignments of SIRT6 and PPARγ with their homologs for conserved or conservatively substituted residues. These include R173, C175, R180, T182, I183, L184, D185, W186, E187, D188, L190, P191, D194, and D206 for SIRT6 and F121, H122, E129, K132, R136, R137, R159, N160, Q163, H177, and R184 for PPARγ. The predicted interfacial residues on PPARγ coincide with DNA-binding residues, adding confidence to our hypothesis that SIRT6 could bind to the DNA-binding region on PPARγ and interferes with the transcription of the fatty acid transporters.

The top docked models from HADDOCK and HDOCK were checked for the restraints that they satisfied. None of the top 10 models from HDOCK could satisfy the restraints; hence, those results were not analyzed further. HADDOCK provides clusters in which models with similar binding poses are grouped together. The best binding pose based on HADDOCK scores and the number of restraints it satisfied are shown in Figures S5D and S5E. The interaction energy was calculated using foldx and was found to be −10.3 kcal/mol (Schymkowitz et al., 2005). No clashes were observed at the interface for this model, and the interface area was found to be 840 Å^2 (calculated using the PDBePISA web service). The interface is small, but the area for transient protein-protein interactions is generally <1,500 Å^2 (Acuner Ozbabacan et al., 2011). The catalytic residues of SIRT6, shown as orange sticks in Figure 5H, were found to be solvent exposed (solvent accessibility ≥7%, calculated from the NACCESS tool) in its complex with PPARγ. This suggests that catalytic residues do not participate in binding with PPARγ and hence explains the ability of catalytically inactive SIRT6 mutants to bind to PPARγ. Further, upon comparison with the RXRα and DNA-bound structure of PPARγ, we observed that the chosen binding pose shows no interference with the RXRα binding and thus is suggestive of competitive binding at only the DNA-binding site of PPARγ (Figures S5D and S5E). These findings

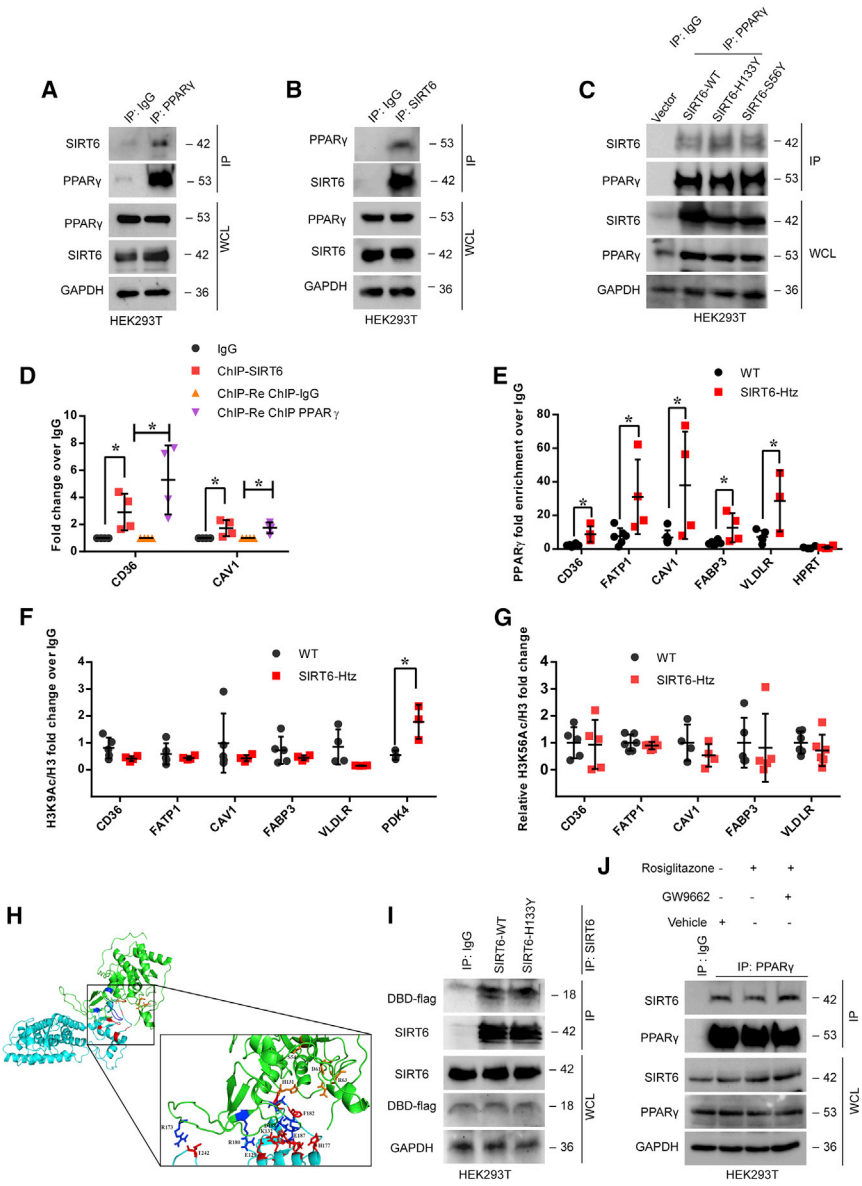

Figure 5. SIRT6 binds to the DNA-binding domain of PPARγ

(A) Co-immunoprecipitation assay showing the interaction of PPARγ and SIRT6. PPARγ was immunoprecipitated from HEK293T cells transfected with PPARγ and SIRT6 plasmids, and the interaction with SIRT6 was tested by immunoblotting. Immunoglobulin G (IgG) was used as a control. Whole-cell lysate (WCL) was probed for indicated proteins by western blotting. n = 3 independent experiments.

(B) SIRT6 was immunoprecipitated, and the interaction with SIRT6 was tested by immunoblotting. IgG was used as a control. WCL was probed for indicated proteins by western blotting. n = 2 independent experiments.

(C) Interaction of PPARγ with WT and catalytic mutants of SIRT6. PPARγ was immunoprecipitated from HEK293T cells transfected with PPARγ along with either SIRT6-WT, SIRT6-H133Y, or SIRT6-S56Y plasmids. Interaction with SIRT6 was assessed by western blotting. IgG was used as a negative control. WCL was probed for indicated proteins by western blotting.

(D) ChIP analysis showing enrichment of PPARγ on the promoter of CD36 and CAV1. Data presented as means ± SDs, n = 4, Student's t test, data are presented as fold IgG, *p < 0.05.

(E) PPARγ binding on the promoters of indicated fatty acid transporters in the heart of WT or SIRT6 heterozygous mice. n = 3–6, Student's t test, data are presented as means ± SDs, *p < 0.05.

(F) Changes in acetylation status at H3K9 residue at the promoter regions of indicated fatty acid transporter genes in the heart of WT and SIRT6 heterozygous mice, n = 3–5 per group. Data are presented as means ± SDs, Student's t test, *p < 0.05.

(G) Acetylation status at H3K56 at the promoter regions of indicated fatty acid transporters genes in the heart of WT and SIRT6 heterozygous mice, n = 4–6 per group. Data are presented as means ± SDs, Student's t test.

(H) Binding of SIRT6 and PPARγ as obtained from the best-scoring HADDOCK model. SIRT6 is shown in green and PPARγ in cyan. Residues defined as restraints for docking are shown in blue and red, respectively. Inset: close-up of the predicted interface is shown (red sticks: PPARγ; blue sticks: SIRT6). The interface includes interactions between the residues used as restraints as well as a few other residues, which have been predicted by docking. Select residues have been labeled, and the numbering is based on the respective crystal structures. The catalytic residues of SIRT6 are shown as orange sticks.

(I) Interaction of SIRT6 with WT and catalytic mutants of SIRT6 with DNA-binding domain of PPARγ. SIRT6 was immunoprecipitated from HEK293T cells transfected with the DNA-binding domain of PPARγ with either SIRT6-WT or SIRT6-H133Y plasmids. Interaction with SIRT6 was assessed by western blotting. IgG was used as a negative control. WCL was probed for indicated proteins by western blotting, n = 3 independent experiments.

(J) Western blot analysis showing the interaction of SIRT6 with PPARγ upon treatment with GW9662 or rosiglitazone. PPARγ was immunoprecipitated from HEK293T cells overexpressing SIRT6 and PPARγ. n = 3 independent experiments.

indicate that SIRT6 may competitively bind to the DNA-binding domain of PPARγ and inhibit its activity by preventing PPARγ from accessing the DNA. Our further co-immunoprecipitation experiments confirmed that SIRT6 interacts with the DNA-binding domain of PPARγ. Consistent with our model prediction, this interaction was independent of the catalytic activity of SIRT6 as SIRT6-H133Y could also bind to the DNA-binding domain of PPARγ (Figure 5I).

From our structural model of PPARγ-SIRT6 complex, we observe that the D188 residue in SIRT6 is involved in an extensive network of interactions at the PPARγ-SIRT6 interface with R136, H122, and K132 of PPARγ (Figure S5F). Notably, D188 is also a highly conserved residue. Hence, we envisaged that mutation of D188 should prevent the binding of PPARγ to SIRT6. To test this, we mutated the key aspartate 188 residue in SIRT6 to alanine and studied the interaction with PPARγ. In

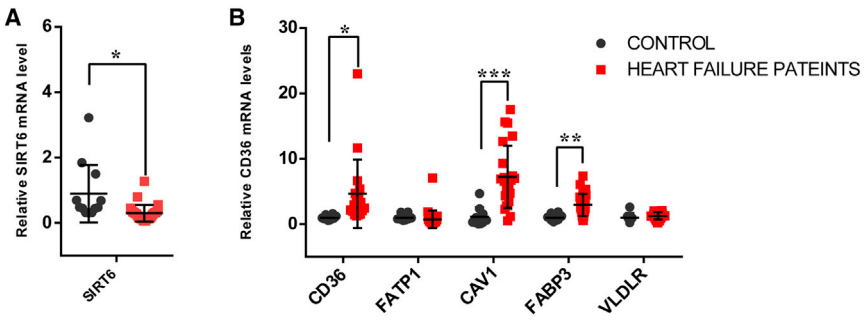

Figure 6. Human failing hearts show low levels of SIRT6

(A) The mRNA levels of SIRT6 in the hearts of control and heart failure patients. Data presented as means ± SDs, n = 12 for controls, n = 28 for heart failure patients, Student's t test, *p < 0.05.

(B) The mRNA levels of fatty acid transporters in the hearts of control and heart failure patients. Data presented as means ± SDs, n = 8–10 for controls, n = 18–26 for heart failure patients, Student's t test, *p < 0.05, **p < 0.005,***p < 0.0005.

our experiments, the D188A mutant SIRT6 exhibited lower-molecular-weight fragments, possibly due to cleavage (Figure S6A). Surprisingly, the D188A SIRT6 mutant was able to interact with PPARγ and also reduced the fatty acid uptake similar to WT SIRT6 and the catalytic mutant (Figures S6B–S6D). We believe that multiple residues of SIRT6 may contribute to its interaction with PPARγ, and further studies are required to identify the residues involved in the interaction of SIRT6 and PPARγ. Studies have shown that PPARγ activators could induce conformational changes leading to the dissociation of its co-repressors, while antagonists such as GW9662 irreversibly block ligand/activator binding to PPARγ, thereby preventing its activation (Leesnitzer et al., 2002; Qiang et al., 2012). Our western blotting analysis suggests that the PPARγ activator did not have any noticeable effect on the interaction between SIRT6 and PPARγ in the presence or absence of the GW9662 (Figure 5J), suggesting that SIRT6-PPARγ interaction is resistant to rosiglitazone/GW9662-induced conformation changes. These findings are in line with our findings that SIRT6 binds to the DNA-binding domain of PPARγ, and agonist induces recruitment/dissociation of interacting partners primarily centered around the ligand-binding domain of PPARγ (Nettles and Greene, 2005).

Human failing hearts show reduced SIRT6 and increased fatty acid transporters

Fatty acid transporters are transcriptionally upregulated in human heart failure patients (Cal et al., 2012; García-Rúa et al., 2012). Therefore, we analyzed the expression of SIRT6 and fatty acid transporters in the left ventricle of these patients. Our analysis suggests that SIRT6 levels significantly downregulated, and the expression of fatty acid transporters, namely CD36, CAV1, and FABP3 but not FATP1 and VLDLR, was increased (Figures 6A and 6B). These findings suggest that SIRT6 may control the expression of fatty acid transporters in human hearts during failure.

DISCUSSION

Excessive accumulation of lipids compromises cardiac function (Goldberg et al., 2012). Although the role of sirtuins in lipid metabolism has been extensively studied, the direct role of sirtuins in regulating the expression of fatty acid transporters and hence the fatty acid uptake have not been studied yet. In the present study, we elucidate a crucial mechanism for SIRT6 in controlling cellular lipid levels by regulating cardiac fatty acid uptake in cardiomyocytes via the PPARγ transcription factor. Importantly, we find that SIRT6 regulates fatty acid uptake, independent of its catalytic activity, similar to our recent report on the effect of SIRT6 in regulating protein synthesis (Ravi et al., 2019).

Calorie restriction extends lifespan and improves cardiac health in higher mammals (Fernández-Ruiz, 2017; Weiss and Fontana, 2011; Yan et al., 2013). Notably, sirtuins have emerged as essential mediators of the benefits of calorie restriction. Multiple sirtuins have been documented to play a vital role in regulating cardiac lipid homeostasis, one of the primary energy sources in the heart (Xu et al., 2016; Zullo et al., 2018). SIRT1 has been shown to both suppress and activate PPARα activity in cardiomyocytes. Notably, the activation of SIRT1 rescues the lipotoxic effects of PPARα and PPARγ activators (Kalliora et al., 2019; Oka et al., 2011; Planavila et al., 2011). The mitochondrial sirtuins SIRT3, SIRT4, and SIRT5 play a direct role in maintaining cardiac lipid homeostasis by affecting the activity of enzymes involved in lipid metabolism by removing their acetyl or fatty-acyl groups. SIRT3KO mice develop cardiac lipotoxicity associated with hyperacetylation of long-chain acyl coenzyme A dehydrogenase (LCAD) (Alrob et al., 2014). Similarly, SIRT5KO mice develop cardiac dysfunction associated with hyper-succinylation and reduction in the activities of key enzymes in the β-oxidation pathway (Sadhukhan et al., 2016). SIRT4 deficiency improves cardiac function and protects from lipid accumulation due to increased fatty acid oxidation (Hoelscher et al., 2017).

Although multiple studies implicate SIRT6 as a critical regulator of metabolism, their role in cardiac metabolism, which is unique in its predominance of lipid metabolism, is somewhat limited. We have previously shown that SIRT6 plays a crucial role in pyruvate oxidation in the heart via the FoxO1 transcription factor (Khan et al., 2018). In the present study, we show that SIRT6 deficiency enhances fatty acid uptake and lipid accumulation in the heart by activating the PPARγ transcription factor. In line with our observations, liver-specific ablation of SIRT6 enhances the uptake of long-chain fatty acids through increased expression of fatty acid translocase (FAT)/CD36 and FAT protein (FATP), leading to the development of fatty liver (Kim et al., 2010). Further, similar to our observations on the regulation of PPARγ by SIRT6, mice overexpressing SIRT6 show reduced expression of a specific set of lipogenic genes under the control of PPARγ in the fat tissue (Kanfi et al., 2010). Moreover, SIRT6 depletion increased PPARγ levels in bovine adipocytes (Hong et al., 2020). We found increased protein levels of PPARγ in SIRT6-deficient mice. However, we do not see any changes in the

mRNA levels of PPARγ isoforms in the heart samples of SIRT6KO mice. This observation indicates that SIRT6 could be regulating PPARγ post-transcriptionally. Studies indicate that PPARγ is regulated by selective proteasomal degradation (Hauser et al., 2000; Kim et al., 2014; Li et al., 2017). Along similar lines, SIRT6 regulates p27 and X-linked inhibitor of apoptosis protein (XIAP) levels by modulating their proteasomal degradation (Zhao et al., 2016; Zhou et al., 2019). In addition, PPARγ mRNA stability is regulated by the action of different microRNAs (miRNAs) (Portius et al., 2017). Notably, SIRT6 also regulates the miRNA levels (Elhanati et al., 2016). Therefore, we believe that SIRT6 may be regulating PPARγ levels through proteasomal degradation or by modulating the miRNAs, although further studies are required to confirm this hypothesis.

In previous work, SIRT6 has been shown to activate the transcription of genes involved in the β-oxidation of fatty acids by acting as a co-activator of PPARα in the liver. SIRT6 may exert tissue-specific and isoform-specific regulation of the PPAR family of transcription factors to control lipid metabolism (Naiman et al., 2019). In addition to PPAR, SIRT6 has been shown to regulate Pparg coactivator 1α (PGC-1α) and FoxO1 transcription factors, which play a crucial role in regulating fatty acid metabolism (Khan et al., 2018; Dominy et al., 2012). It is, therefore, possible that SIRT6 could regulate lipid metabolism through multiple transcription factors. Further, the increased fat accumulation in the heart and liver of SIRT6-deficient mice may be due to the combined effect of increased fatty acid uptake and reduced fatty acid oxidation.

The rate of fatty acid uptake in the heart is mediated by fatty acid transporters (van der Vusse et al., 2000). An increase in fatty acid transporter level leads to the accumulation of lipids in the heart and then to lipotoxicity (Koonen et al., 2007). Notably, mice deficient for myocardial FAT/CD36 show reduced fatty acid uptake rates and protection against cardiac lipotoxicity (Yang et al., 2007). Further, in metabolic disease models such as the diabetic animal models, there is an imbalance between fatty acid uptake and fatty acid oxidation in the heart (Bayeva et al., 2013). In line with these observations, we also find a similar phenotype in *db/db* diabetic mice, in which most of the fatty acid transporters upregulated while the levels of SIRT6 are lower. The increased myocardial lipid accumulation, in turn, causes lipotoxicity, which then leads to the development of cardiac dysfunction. Since failing hearts show defective fatty acid utilization, a sustained increase in fatty acid uptake could further exacerbate heart failure.

Our studies show a crucial role for SIRT6 in regulating lipid levels in the heart through transcriptional control of fatty acid transporters. Our observations suggest that targeting SIRT6 and increasing its expression may be beneficial in reducing cardiac lipotoxicity. Recent studies have shown that expression of SIRT6 can be enhanced by calorie restriction or by treatment with lycorine hydrochloride (Hernández-Saavedra et al., 2021; Zhang et al., 2021). Therefore, SIRT6 could be a therapeutic target for metabolic diseases affecting the heart.

STAR★METHODS

Detailed methods are provided in the online version of this paper and include the following:

SUPPLEMENTAL INFORMATION

Supplemental information can be found online at https://doi.org/10.1016/j.celrep.2021.109190.

ACKNOWLEDGMENTS

The central animal facility, central confocal facility (Division of Biological Sciences and Department of Microbiology and Cell Biology), flow cytometry facility, and the microtome facility (Division of Biological Sciences), Indian Institute of Science, Bengaluru, are acknowledged for their services and the technical help. This work is supported by funding from the Department of Science and Technology (EMR/2014/000065, CRG/2018/000699), Department of Biotechnology (BRB/10/1294/2014, MED/30/1454/2014), Council for Scientific and Industrial Research (37(1646)/15/EMR-II), and the Department of Biotechnology–Indian Institute of Science partnership program for advanced research. R.M. is supported by NIH grants R01GM128448 and R33ES025638. N.R.S. is a recipient of the Innovative Young Biotechnologist Award (IYBA), the National Bioscience Award for Career Development, and the Ramalingaswami Re-entry Fellowship from the Department of Biotechnology, Government of India. N.A.-J. is a DST-INSPIRE faulty fellow. N.S. is a J.C. Bose National Fellow. H.T. was supported by a studentship from DST-INSPIRE. J.P. is supported by the Prime Minister's Research Fellowship (PMRF). N.S. acknowledges support from the Bioinformatics and Computational Biology Centre, Department of Biotechnology (DBT).

AUTHOR CONTRIBUTIONS

N.R.S. conceived, designed, and supervised the study and wrote the final draft of the manuscript. D.K. and T.A. designed and analyzed the experiments and performed the primary cardiomyocyte culture, animal experiments, qPCR, co-immunoprecipitation and ChIP and confocal microscopy. D.K. and S.D.

performed the flow cytometry experiments. D.K., T.A., V.R., S.M., and A.S.B. performed the immunoblotting. N.S. conceived and designed the computational structural analyses. H.T. and J.P. performed the computational analyses and the molecular docking experiments. H.T. wrote the results for the computational structural analysis experiments. A.K.T. performed and analyzed the HFD qPCR experiments. N.A.-J. performed the oil red O staining. E.A.G., J.-P.E., and R.M. analyzed the ChIP-seq and RNA-seq experiments. S.K. performed the bioinformatic analysis. U.K.-S. provided the SIRT6KO mice. U.K.-S. and R.M. were involved in the project discussions. T.A. and A.S.B. quantified the confocal images. S.R. performed the luciferase reporter assays. A.S.B. and R.R. performed the genotyping of the SIRT6 heterozygous and *db/db* mice. R.R. performed the site-directed mutagenesis and H3K56Ac ChIP. R.R. and S.R. generated the CD36 promoter-luciferase construct. P.S.M.R. recruited the patients and collected the human heart tissues. V.R., D.K., and T.A. wrote the manuscript. Original data have been cross-verified by S.R., S.M., and N.R.S.

DECLARATION OF INTERESTS

The authors declare no competing interests.

Received: July 9, 2020
Revised: March 8, 2021
Accepted: May 7, 2021
Published: June 1, 2021

REFERENCES

Acuner Ozbabacan, S.E., Engin, H.B., Gursoy, A., and Keskin, O. (2011). Transient protein-protein interactions. Protein Eng. Des. Sel. *24*, 635–648.

Alrob, O.A., Sankaralingam, S., Ma, C., Wagg, C.S., Fillmore, N., Jaswal, J.S., Sack, M.N., Lehner, R., Gupta, M.P., Michelakis, E.D., et al. (2014). Obesity-induced lysine acetylation increases cardiac fatty acid oxidation and impairs insulin signalling. Cardiovasc. Res. *103*, 485–497.

Aprile, M., Cataldi, S., Ambrosio, M.R., D'Esposito, V., Lim, K., Dietrich, A., Blüher, M., Savage, D.B., Formisano, P., Ciccodicola, A., et al. (2018). PPARγ-Δ5, a Naturally Occurring Dominant-Negative Splice Isoform, Impairs PPARγ Function and Adipocyte Differentiation. Cell reports *25*, 1577–1592.e1576.

Ashkenazy, H., Abadi, S., Martz, E., Chay, O., Mayrose, I., Pupko, T., and Ben-Tal, N. (2016). ConSurf 2016: an improved methodology to estimate and visualize evolutionary conservation in macromolecules. Nucleic Acids Res. *44* (*W1*), W344–W350.

Auwerx, J. (1999). PPARgamma, the ultimate thrifty gene. Diabetologia *42*, 1033–1049.

Bayeva, M., Sawicki, K.T., and Ardehali, H. (2013). Taking diabetes to heart–deregulation of myocardial lipid metabolism in diabetic cardiomyopathy. J. Am. Heart Assoc. *2*, e000433.

Berman, H.M., Westbrook, J., Feng, Z., Gilliland, G., Bhat, T.N., Weissig, H., Shindyalov, I.N., and Bourne, P.E. (2000). The Protein Data Bank. Nucleic Acids Res. *28*, 235–242.

Bertero, E., and Maack, C. (2018). Metabolic remodelling in heart failure. Nat. Rev. Cardiol. *15*, 457–470.

Bonen, A., Luiken, J.J.F.P., and Glatz, J.F.C. (2002). Regulation of fatty acid transport and membrane transporters in health and disease. Mol. Cell. Biochem. *239*, 181–192.

Braissant, O., Foufelle, F., Scotto, C., Dauça, M., and Wahli, W. (1996). Differential expression of peroxisome proliferator-activated receptors (PPARs): tissue distribution of PPAR-alpha, -beta, and -gamma in the adult rat. Endocrinology *137*, 354–366.

Cal, R., Juan-Babot, O., Brossa, V., Roura, S., Gálvez-Montón, C., Portoles, M., Rivera, M., Cinca, J., Badimon, L., and Llorente-Cortés, V. (2012). Low density lipoprotein receptor-related protein 1 expression correlates with cholesteryl ester accumulation in the myocardium of ischemic cardiomyopathy patients. J. Transl. Med. *10*, 160.

Chabowski, A., Górski, J., Glatz, J.F.C., Luiken, J.F.P., and Bonen, A. (2008). Protein-mediated Fatty Acid Uptake in the Heart. Curr. Cardiol. Rev. *4*, 12–21.

Chandra, V., Huang, P., Hamuro, Y., Raghuram, S., Wang, Y., Burris, T.P., and Rastinejad, F. (2008). Structure of the intact PPAR-gamma-RXR- nuclear receptor complex on DNA. Nature *456*, 350–356.

Chiu, H.-C., Kovacs, A., Blanton, R.M., Han, X., Courtois, M., Weinheimer, C.J., Yamada, K.A., Brunet, S., Xu, H., Nerbonne, J.M., et al. (2005). Transgenic Expression of Fatty Acid Transport Protein 1 in the Heart Causes Lipotoxic Cardiomyopathy. Circ. Res. *96*, 225–233.

Coleman, D.L., and Hummel, K.P. (1967). Studies with the mutation, diabetes, in the mouse. Diabetologia *3*, 238–248.

Cotney, J.L., and Noonan, J.P. (2015). Chromatin immunoprecipitation with fixed animal tissues and preparation for high-throughput sequencing. Cold Spring Harb. Protoc. *2015*, 419.

Dominy, J.E., Jr., Lee, Y., Jedrychowski, M.P., Chim, H., Jurczak, M.J., Camporez, J.P., Ruan, H.B., Feldman, J., Pierce, K., Mostoslavsky, R., et al. (2012). The deacetylase Sirt6 activates the acetyltransferase GCN5 and suppresses hepatic gluconeogenesis. Mol. Cell *48*, 900–913.

Drosatos, K., and Schulze, P.C. (2013). Cardiac lipotoxicity: molecular pathways and therapeutic implications. Curr. Heart Fail. Rep. *10*, 109–121.

Dunham, I., Kundaje, A., Aldred, S.F., Collins, P.J., Davis, C.A., Doyle, F., Epstein, C.B., Frietze, S., Harrow, J., Kaul, R., et al.; ENCODE Project Consortium (2012). An integrated encyclopedia of DNA elements in the human genome. Nature *489*, 57–74.

Elhanati, S., Kanfi, Y., Varvak, A., Roichman, A., Carmel-Gross, I., Barth, S., Gibor, G., and Cohen, H.Y. (2013). Multiple regulatory layers of SREBP1/2 by SIRT6. Cell Rep. *4*, 905–912.

Elhanati, S., Ben-Hamo, R., Kanfi, Y., Varvak, A., Glazz, R., Lerrer, B., Efroni, S., and Cohen, H.Y. (2016). Reciprocal Regulation between SIRT6 and miR-122 Controls Liver Metabolism and Predicts Hepatocarcinoma Prognosis. Cell Rep. *14*, 234–242.

Etchegaray, J.-P., Zhong, L., Li, C., Henriques, T., Ablondi, E., Nakadai, T., Van Rechem, C., Ferrer, C., Ross, K.N., Choi, J.-E., et al. (2019). The Histone Deacetylase SIRT6 Restrains Transcription Elongation via Promoter-Proximal Pausing. Mol. Cell *75*, 683–699.e7.

Feldman, J.L., Dittenhafer-Reed, K.E., and Denu, J.M. (2012). Sirtuin catalysis and regulation. J. Biol. Chem. *287*, 42419–42427.

Fernández-Ruiz, I. (2017). Metabolism: calorie restriction for healthy ageing. Nat. Rev. Cardiol. *14*, 190.

Finn, R.D., Clements, J., and Eddy, S.R. (2011). HMMER web server: interactive sequence similarity searching. Nucleic Acids Res. *39*, W29–W37.

Fiser, A., and Sali, A. (2003). ModLoop: automated modeling of loops in protein structures. Bioinformatics *19*, 2500–2501.

García-Rúa, V., Otero, M.F., Lear, P.V., Rodríguez-Penas, D., Feijóo-Bandín, S., Noguera-Moreno, T., Calaza, M., Álvarez-Barredo, M., Mosquera-Leal, A., Parrington, J., et al. (2012). Increased expression of fatty-acid and calcium metabolism genes in failing human heart. PLoS ONE *7*, e37505.

Glatz, J.F.C., Luiken, J.J.F.P., and Bonen, A. (2010). Membrane fatty acid transporters as regulators of lipid metabolism: implications for metabolic disease. Physiol. Rev. *90*, 367–417.

Glatz, J.F.C., Angin, Y., Steinbusch, L.K.M., Schwenk, R.W., and Luiken, J.J.F.P. (2013). CD36 as a target to prevent cardiac lipotoxicity and insulin resistance. Prostaglandins Leukot. Essent. Fatty Acids *88*, 71–77.

Goldberg, I.J., Trent, C.M., and Schulze, P.C. (2012). Lipid metabolism and toxicity in the heart. Cell Metab. *15*, 805–812.

Hauser, S., Adelmant, G., Sarraf, P., Wright, H.M., Mueller, E., and Spiegelman, B.M. (2000). Degradation of the peroxisome proliferator-activated receptor γ is linked to ligand-dependent activation. J. Biol. Chem. *275*, 18527–18533.

Herman-Edelstein, M., Scherzer, P., Tobar, A., Levi, M., and Gafter, U. (2014). Altered renal lipid metabolism and renal lipid accumulation in human diabetic nephropathy. J. Lipid Res. *55*, 561–572.

Hernández-Saavedra, D., Moody, L., Tang, X., Goldberg, Z.J., Wang, A.P., Chen, H., and Pan, Y.X. (2021). Caloric restriction following early-life high fat-diet feeding represses skeletal muscle TNF in male rats. J. Nutr. Biochem. *91*, 108598.

Hoelscher, M.E., Koentges, C., Muesse, C., Birkle, S., Hoffmann, M.M., Bode, C., and Bugger, H. (2017). P2095SIRT4 regulates fatty acid utilisation and cardiac function in the normal and diabetic heart. Eur. Heart J. *38* (*Suppl 1*), ehx502.P2095.

Hong, J., Mei, C., Abbas Raza, S.H., Khan, R., Cheng, G., and Zan, L. (2020). SIRT6 cooperates with SIRT5 to regulate bovine preadipocyte differentiation and lipid metabolism via the AMPKα signaling pathway. Arch. Biochem. Biophys. *681*, 108260.

Houtkooper, R.H., Pirinen, E., and Auwerx, J. (2012). Sirtuins as regulators of metabolism and healthspan. Nat. Rev. Mol. Cell Biol. *13*, 225–238.

Jain, A., Ravi, V., Muhamed, J., Chatterjee, K., and Sundaresan, N.R. (2017). A simplified protocol for culture of murine neonatal cardiomyocytes on nanoscale keratin coated surfaces. Int. J. Cardiol. *232*, 160–170.

Kalliora, C., Kyriazis, I.D., Oka, S.-i., Lieu, M.J., Yue, Y., Area-Gomez, E., Pol, C.J., Tian, Y., Mizushima, W., Chin, A., et al. (2019). Dual PPARα/γ activation inhibits SIRT1-PGC1α axis and causes cardiac dysfunction. JCI Insight *4*, e129556.

Kanfi, Y., Peshti, V., Gil, R., Naiman, S., Nahum, L., Levin, E., Kronfeld-Schor, N., and Cohen, H.Y. (2010). SIRT6 protects against pathological damage caused by diet-induced obesity. Aging Cell *9*, 162–173.

Katoh, K., and Standley, D.M. (2014). MAFFT: iterative refinement and additional methods. Methods Mol. Biol. *1079*, 131–146.

Khan, D., Sarikhani, M., Dasgupta, S., Maniyadath, B., Pandit, A.S., Mishra, S., Ahamed, F., Dubey, A., Fathma, N., Atreya, H.S., et al. (2018). SIRT6 deacetylase transcriptionally regulates glucose metabolism in heart. J. Cell. Physiol. *233*, 5478–5489.

Kim, H.S., Xiao, C., Wang, R.H., Lahusen, T., Xu, X., Vassilopoulos, A., Vazquez-Ortiz, G., Jeong, W.I., Park, O., Ki, S.H., et al. (2010). Hepatic-specific disruption of SIRT6 in mice results in fatty liver formation due to enhanced glycolysis and triglyceride synthesis. Cell Metab. *12*, 224–236.

Kim, J.H., Park, K.W., Lee, E.W., Jang, W.S., Seo, J., Shin, S., Hwang, K.A., and Song, J. (2014). Suppression of PPARγ through MKRN1-mediated ubiquitination and degradation prevents adipocyte differentiation. Cell Death Differ. *21*, 594–603.

Koonen, D.P., Febbraio, M., Bonnet, S., Nagendran, J., Young, M.E., Michelakis, E.D., and Dyck, J.R. (2007). CD36 expression contributes to age-induced cardiomyopathy in mice. Circulation *116*, 2139–2147.

Kugel, S., and Mostoslavsky, R. (2014). Chromatin and beyond: the multitasking roles for SIRT6. Trends Biochem. Sci. *39*, 72–81.

Lee, C., and Huang, C.-H. (2013). LASAGNA-Search: an integrated web tool for transcription factor binding site search and visualization. Biotechniques *54*, 141–153.

Lee, W.-S., and Kim, J. (2015). Peroxisome Proliferator-Activated Receptors and the Heart: Lessons from the Past and Future Directions. PPAR Res. *2015*, 271983.

Leesnitzer, L.M., Parks, D.J., Bledsoe, R.K., Cobb, J.E., Collins, J.L., Consler, T.G., Davis, R.G., Hull-Ryde, E.A., Lenhard, J.M., Patel, L., et al. (2002). Functional consequences of cysteine modification in the ligand binding sites of peroxisome proliferator activated receptors by GW9662. Biochemistry *41*, 6640–6650.

Li, P., Song, Y., Zan, W., Qin, L., Han, S., Jiang, B., Dou, H., Shao, C., and Gong, Y. (2017). Lack of CUL4B in Adipocytes Promotes PPARα-Mediated Adipose Tissue Expansion and Insulin Sensitivity. Diabetes *66*, 300–313.

Motojima, K., Passilly, P., Peters, J.M., Gonzalez, F.J., and Latruffe, N. (1998). Expression of Putative Fatty Acid Transporter Genes Are Regulated by Peroxisome Proliferator-activated Receptor Alpha and Gamma Activators in a Tissue- and Inducer-specific Manner. J. Biol. Chem. *273*, 16710–16714.

Naiman, S., Huynh, F.K., Gil, R., Glick, Y., Shahar, Y., Touitou, N., Nahum, L., Avivi, M.Y., Roichman, A., Kanfi, Y., et al. (2019). SIRT6 Promotes Hepatic Beta-Oxidation via Activation of PPARα. Cell Rep. *29*, 4127–4143.e8.

Nettles, K.W., and Greene, G.L. (2005). Ligand control of coregulator recruitment to nuclear receptors. Annu. Rev. Physiol. *67*, 309–333.

North, B.J., Marshall, B.L., Borra, M.T., Denu, J.M., and Verdin, E. (2003). The human Sir2 ortholog, SIRT2, is an NAD+-dependent tubulin deacetylase. Mol. Cell *11*, 437–444.

Oka, S., Alcendor, R., Zhai, P., Park, J.Y., Shao, D., Cho, J., Yamamoto, T., Tian, B., and Sadoshima, J. (2011). PPARα-Sirt1 complex mediates cardiac hypertrophy and failure through suppression of the ERR transcriptional pathway. Cell Metab. *14*, 598–611.

Pan, P.W., Feldman, J.L., Devries, M.K., Dong, A., Edwards, A.M., and Denu, J.M. (2011). Structure and Biochemical Functions of SIRT6. J. Biol. Chem. *286*, 14575–14587.

Perman, J.C., Boström, P., Lindbom, M., Lidberg, U., Ståhlman, M., Hägg, D., Lindskog, H., Scharin Täng, M., Omerovic, E., Mattsson Hultén, L., et al. (2011). The VLDL receptor promotes lipotoxicity and increases mortality in mice following an acute myocardial infarction. J. Clin. Invest. *121*, 2625–2640.

Planavila, A., Iglesias, R., Giralt, M., and Villarroya, F. (2011). Sirt1 acts in association with PPARα to protect the heart from hypertrophy, metabolic dysregulation, and inflammation. Cardiovasc. Res. *90*, 276–284.

Portius, D., Sobolewski, C., and Foti, M. (2017). MicroRNAs-Dependent Regulation of PPARs in Metabolic Diseases and Cancers. PPAR Res. *2017*, 7058424.

Qiang, L., Wang, L., Kon, N., Zhao, W., Lee, S., Zhang, Y., Rosenbaum, M., Zhao, Y., Gu, W., Farmer, S.R., and Accili, D. (2012). Brown remodeling of white adipose tissue by SirT1-dependent deacetylation of Pparγ. Cell *150*, 620–632.

Rao, M.S., Papreddy, K., Musunuri, S., and Okonkwo, A. (2002). Prevention/reversal of choline deficiency-induced steatohepatitis by a peroxisome proliferator-activated receptor alpha ligand in rats. In Vivo *16*, 145–152.

Ravi, V., Jain, A., Khan, D., Ahamed, F., Mishra, S., Giri, M., Inbaraj, M., Krishna, S., Sarikhani, M., Maity, S., et al. (2019). SIRT6 transcriptionally regulates global protein synthesis through transcription factor Sp1 independent of its deacetylase activity. Nucleic Acids Res. *47*, 9115–9131.

Sadhukhan, S., Liu, X., Ryu, D., Nelson, O.D., Stupinski, J.A., Li, Z., Chen, W., Zhang, S., Weiss, R.S., Locasale, J.W., et al. (2016). Metabolomics-assisted proteomics identifies succinylation and SIRT5 as important regulators of cardiac function. Proc. Natl. Acad. Sci. USA *113*, 4320–4325.

Schaiff, W.T., Bildirici, I., Cheong, M., Chern, P.L., Nelson, D.M., and Sadovsky, Y. (2005). Peroxisome Proliferator-Activated Receptor-γ and Retinoid X Receptor Signaling Regulate Fatty Acid Uptake by Primary Human Placental Trophoblasts. The Journal of Clinical Endocrinology & Metabolism *90*, 4267–4275.

Schneider, C.A., Rasband, W.S., and Eliceiri, K.W. (2012). NIH Image to ImageJ: 25 years of image analysis. Nat. Methods *9*, 671–675.

Schulze, P.C., Drosatos, K., and Goldberg, I.J. (2016). Lipid Use and Misuse by the Heart. Circ. Res. *118*, 1736–1751.

Schymkowitz, J., Borg, J., Stricher, F., Nys, R., Rousseau, F., and Serrano, L. (2005). The FoldX web server: an online force field. Nucleic Acids Res. *33*, W382–W388.

Sebastián, C., Zwaans, B.M., Silberman, D.M., Gymrek, M., Goren, A., Zhong, L., Ram, O., Truelove, J., Guimaraes, A.R., Toiber, D., et al. (2012). The histone deacetylase SIRT6 is a tumor suppressor that controls cancer metabolism. Cell *151*, 1185–1199.

Shan, T.Z., Ren, Y., Wu, T., Liu, C.X., and Wang, Y.Z. (2009). Regulatory role of Sirt1 on the gene expression of fatty acid-binding protein 3 in cultured porcine adipocytes. J. Cell. Biochem. *107*, 984–991.

Son, N.-H., Park, T.-S., Yamashita, H., Yokoyama, M., Huggins, L.A., Okajima, K., Homma, S., Szabolcs, M.J., Huang, L.-S., and Goldberg, I.J. (2007).

Cardiomyocyte expression of PPARgamma leads to cardiac dysfunction in mice. J. Clin. Invest. *117*, 2791–2801.

Sundaresan, N.R., Vasudevan, P., Zhong, L., Kim, G., Samant, S., Parekh, V., Pillai, V.B., Ravindra, P.V., Gupta, M., Jeevanandam, V., et al. (2012). The sirtuin SIRT6 blocks IGF-Akt signaling and development of cardiac hypertrophy by targeting c-Jun. Nat. Med. *18*, 1643–1650.

Tina, K.G., Bhadra, R., and Srinivasan, N. (2007). PIC: Protein Interactions Calculator. Nucleic Acids Res. *35*, W473–W476.

van der Vusse, G.J., van Bilsen, M., and Glatz, J.F.C. (2000). Cardiac fatty acid uptake and transport in health and disease. Cardiovasc. Res. *45*, 279–293.

van Zundert, G.C.P., Rodrigues, J.P.G.L.M., Trellet, M., Schmitz, C., Kastritis, P.L., Karaca, E., Melquiond, A.S.J., van Dijk, M., de Vries, S.J., and Bonvin, A.M.J.J. (2016). The HADDOCK2.2 Web Server: User-Friendly Integrative Modeling of Biomolecular Complexes. J. Mol. Biol. *428*, 720–725.

Weiss, E.P., and Fontana, L. (2011). Caloric restriction: powerful protection for the aging heart and vasculature. Am. J. Physiol Heart Circ. Physiol. *301*, H1205–H1219.

Xu, S., Bai, P., and Jin, Z.G. (2016). Sirtuins in Cardiovascular Health and Diseases. Trends Endocrinol. Metab. *27*, 677–678.

Yan, L., Gao, S., Ho, D., Park, M., Ge, H., Wang, C., Tian, Y., Lai, L., De Lorenzo, M.S., Vatner, D.E., and Vatner, S.F. (2013). Calorie restriction can reverse, as well as prevent, aging cardiomyopathy. Age (Dordr.) *35*, 2177–2182.

Yan, Y., Zhang, D., Zhou, P., Li, B., and Huang, S.-Y. (2017). HDOCK: a web server for protein-protein and protein-DNA/RNA docking based on a hybrid strategy. Nucleic Acids Res. *45* (*W1*), W365–W373.

Yang, J., Sambandam, N., Han, X., Gross, R.W., Courtois, M., Kovacs, A., Febbraio, M., Finck, B.N., and Kelly, D.P. (2007). CD36 deficiency rescues lipotoxic cardiomyopathy. Circ. Res. *100*, 1208–1217.

Zhang, W., Yang, J., Chen, Y., Xue, R., Mao, Z., Lu, W., and Jiang, Y. (2021). Lycorine hydrochloride suppresses stress-induced premature cellular senescence by stabilizing the genome of human cells. Aging Cell *20*, e13307.

Zhao, G., Wang, H., Xu, C., Wang, P., Chen, J., Wang, P., Sun, Z., Su, Y., Wang, Z., Han, L., and Tong, T. (2016). SIRT6 delays cellular senescence by promoting p27Kip1 ubiquitin-proteasome degradation. Aging (Albany NY) *8*, 2308–2323.

Zhong, L., D'Urso, A., Toiber, D., Sebastian, C., Henry, R.E., Vadysirisack, D.D., Guimaraes, A., Marinelli, B., Wikstrom, J.D., Nir, T., et al. (2010). The histone deacetylase Sirt6 regulates glucose homeostasis via Hif1α. Cell *140*, 280–293.

Zhou, H.-Z., Zeng, H.-Q., Yuan, D., Ren, J.-H., Cheng, S.-T., Yu, H.-B., Ren, F., Wang, Q., Qin, Y.-P., Huang, A.-L., and Chen, J. (2019). NQO1 potentiates apoptosis evasion and upregulates XIAP via inhibiting proteasome-mediated degradation SIRT6 in hepatocellular carcinoma. Cell Commun. Signal. *17*, 168.

Zullo, A., Simone, E., Grimaldi, M., Musto, V., and Mancini, F.P. (2018). Sirtuins as Mediator of the Anti-Ageing Effects of Calorie Restriction in Skeletal and Cardiac Muscle. Int. J. Mol. Sci. *19*, 928.

STAR★METHODS

KEY RESOURCES TABLE

REAGENT or RESOURCE	SOURCE	IDENTIFIER
Antibodies		
CD36 (western blotting)	Abcam	Cat# Ab133625, RRID:AB_2716564
CD36 (confocal microscopy)	Santa Cruz Biotechnology	Cat# Sc7309, RRID:AB_627044
CAV1	CLOUD-CLONE	Cat# PAA214Mu01
FABP3	Abcam	Cat# Ab16916, RRID:AB_443553
PPAR	Cell Signaling Technology	Cat# 2443, RRID:AB_823598
PPAR	Santa Cruz Biotechnology	Cat# Sc7273, RRID:AB_628115
GAPDH	Sigma	Cat# G9545, RRID:AB_796208
Tubulin	Santa Cruz Biotechnology	Cat# Sc8035, RRID:AB_628408
SIRT6	Cell Signaling Technology	Cat# 12486, RRID:AB_2636969
VLDLR	Santa Cruz Biotechnology	Cat# Sc18824, RRID:AB_2216805
H3	Cell Signaling Technology	Cat# 4260, RRID:AB_1904005
H3K9AC	Cell Signaling Technology	Cat# 9649, RRID:AB_823528
Acetylated lysine	Cell Signaling Technology	Cat# 9681s, RRID:AB_331799
Acetylated lysine	Cell Signaling Technology	Cat# 9814s, RRID:AB_10544700
H3K56AC	Millipore	Cat# 07-677-1, RRID:AB_390167
FLAG	Sigma	Cat# F7425, RRID:AB_439687
anti-rabbit HRP	Cell Signaling Technology	Cat# 7074, RRID:AB_2099233
anti-mouse HRP	Cell Signaling Technology	Cat# 7076, RRID:AB_330924
Normal rabbit IgG	Cell Signaling Technology	Cat# 2729, RRID:AB_1031062
Donkey anti-mouse, alexa fluor 488	Thermo Fisher Scientific	Cat# A-21202, RRID:AB_141607
Goat anti-rabbit, alexa fluor 546	Thermo Fisher Scientific	Cat# A-11035, RRID:AB_143051
Clean-blot IP detection reagent	Thermo Fisher Scientific	Cat# 21230, RRID:AB_2864363
Bacterial and virus strains		
Ad null	Vector Biolab	Cat# 1300
Ad-SIRT6 (human)	Vector Biolab, Adenovirus	Cat# 1556
Chemicals, peptides, and recombinant proteins		
Hoechst 33342	Thermo Fisher Scientific	Cat# H3570
BODIPY-C1,C-12	Thermo fisher Scientific	Cat# D3823
BODIPY $^{493/503}$	Thermo fisher Scientific	Cat# D3922
GW9662	Cayman	Cat# 70785
Rosiglitazone	Sigma-Aldrich	Cat# 122320-73-4
Complete, mini protease inhibitor Cocktail	Sigma-Aldrich	Cat# 11836170001
Critical commercial assays		
Clarity ECL western blotting substrate	BioRad	Cat# 1705061
Clarity max western ECL substrate	BioRad	Cat# 1705062
Surebeads protein G	BioRad	Cat# 161-4023 S
Protein G magnetic beads	Cell Signaling Technology	Cat# 70024s
cDNA synthesis kit	BioRad	Cat# 1708890
SYBR green-PCR mix	BioRad	Cat# 1725121
SYBR green-PCR mix	TAKARA	Cat# RR820
Lipofectamine 2000 transfection reagent	Thermo Fisher Scientific	Cat# 11668019
Lipofectamine RNAiMAX transfection reagent	Thermo Fisher Scientific	Cat# 13778150
Lipofectamine 3000 transfection reagent	Thermo Fisher Scientific	Cat# L3000015

(*Continued on next page*)

Continued

REAGENT or RESOURCE	SOURCE	IDENTIFIER
Horse serum, heat inactivated	Thermo Fisher Scientific	Cat# 26050088
Fetal bovine serum	Thermo Fisher Scientific	Cat# 10500064
Antibiotic-Antimycotic mixture	Thermo Fisher Scientific	Cat# 15240062
ProLong gold antifade mountant with DAPI	Thermo Fisher Scientific	Cat# P36931
Deposited data		
RNA-Seq	Etchegaray et al., 2019	GEO: GSE130690
ChIP-Seq	Etchegaray et al., 2019	GEO: GSE130689
ChIP-Seq -K562 Cells	Dunham et al., 2012	ENCSR000AUB
ChIP-Seq -H1 Cells	Dunham et al., 2012	ENCSR000AUS
SIRT6 structure	Pan et al., 2011	3pki
PPARg structure	Chandra et al., 2008	3e00
Human reference genome NCBI build 37, GRCh37	Genome Reference Consortium	https://www.ncbi.nlm.nih.gov/grc/human
Experimental models: cell lines		
HEK293T	ATCC	Cat# CRL-3216, RRID:CVCL_0063
HeLa	ATCC	Cat# CRM-CCL-2, RRID:CVCL_0030
Experimental models: organisms/strains		
Mouse: SIRT6 ±	The Jackson Laboratory	RRID:IMSR_JAX:006050
Mouse: db/db	The Jackson Laboratory	RRID:IMSR_JAX:000697
Mouse: C57BL/6J	The Jackson Laboratory	RRID:IMSR_JAX:000664
Oligonucleotides		
Primer sequences	Please see Table S2	N/A
SIRT6 siRNA (RAT) GCAUCUCAAUGGUUCCUAU	Ravi et al., 2019	N/A
SIRT6 siRNA (Human) AAGAAUGUGCCAAGUGUAAGA	Ravi et al., 2019	N/A
Control siRNA AAUUCUCCGAACGUGUCACGU	Ravi et al., 2019	N/A
Recombinant DNA		
SIRT6 Flag	North et al., 2003	Addgene Cat #13817, RRID:AB_13817
SIRT6 Flag-H133Y	Ravi et al., 2019	N/A
SIRT6 Flag-S56Y	Ravi et al., 2019	N/A
SIRT6 Flag-D188A	This study	N/A
Pparg Flag	Hauser et al., 2000	Addgene Cat# 8895, RRID:AB_8895
Pparg DNA binding domain flag	This study	N/A
Cd36 promoter luciferase	This study	N/A
Software and algorithms		
ImageJ	Schneider et al., 2012	https://imagej.nih.gov/ij/
CONSURF	Ashkenazy et al., 2016	https://consurf.tau.ac.il/
HADDOCK	van Zundert et al., 2016	https://wenmr.science.uu.nl/
HDOCK	Yan et al., 2017	http://hdock.phys.hust.edu.cn/
ModLoop	Fiser and Sali, 2003	https://modbase.compbio.ucsf.edu/modloop/
FoldX	Schymkowitz et al., 2005	http://foldxsuite.crg.eu/
Lasagna	Lee and Huang, 2013	https://biogrid-lasagna.engr.uconn.edu/lasagna_search/index.php
Other		
ChemiDoc touch imaging system	BioRad	N/A
QuantStudio 6 flex RealTime PCR system	Thermo Fisher Scientific	N/A
LSM 880 confocal microscope	Carl Zeiss	N/A
BIORUPTOR PICO	DIAGENODE	N/A
Hybond PVDF membrane	Amersham	N/A

RESOURCE AVAILABILITY

Lead contact

Further information and requests for resources and reagents should be directed to and will be fulfilled by the Lead Contact N. Ravi Sundaresan (rsundaresan@iisc.ac.in).

Materials availability

All unique/stable reagents generated in this study are available from the Lead Contact with a completed Materials Transfer Agreement.

Data and code availability

This study did not generate any unique datasets or code. The source data for figures in the paper are available from the Lead Contact on request.

EXPERIMENTAL MODEL AND SUBJECT DETAILS

Cell culture and plasmids

HEK293T cells were cultured in Dulbecco's Modified Eagle Media (DMEM) supplemented with 10% fetal bovine serum (FBS) at 37°C and 5% CO_2. For transfection, cells were seeded up to 80% confluence, and the plasmids were transfected using Lipofectamine® 2000 according to the manufacturer's protocol. For the transfection of siRNAs, Lipofectamine RNAiMAX was used as per the manufacturer's protocol. Primary cardiomyocytes were cultured from neonatal rat pups as described in our previous study (Jain et al., 2017). Briefly, the pups were sacrificed, and the heart was collected in phosphate buffer saline with glucose. The heart tissues were then minced and digested with 0.2% trypsin and collagenase II. The digestion was carried out for multiple rounds, and the supernatant containing the cells was collected in horse serum after each step. The cells were then pre-plated on a 100mm dish for 45 minutes for the removal of fibroblasts. The unattached cardiomyocytes from these plates were then collected and seeded into fresh culture plates coated with 0.2% gelatin. Transfection of cardiomyocytes with plasmids was performed using Lipofectamine® 3000 as per manufacturer's guidelines. SIRT6 reconstitution experiments were performed in cardiomyocytes by transfecting them first with SIRT6 specific siRNA for 60 hours, followed by transfection with SIRT6 plasmid construct. The cells were harvested 36 hours post-transfection with SIRT6 plasmids. CD36 promoter region was cloned into pGL3 basic vector as per standard protocols. The DNA binding domain of PPARγ was cloned using the services of Genescript, U.S.A. The fragment corresponding to this domain (amino acids 111 to 223 of PPARγ) was obtained from the full-length PPARγ-Flag plasmid (Addgene #8895) and cloned in pCDNA vector along with a flag tag at the C terminus.

Animal experiments

All experiments involving animals were performed in strict accordance with the Institute's Committee for the Purpose of Control and Supervision of Experiments on Animals (CPCSEA), Government of India. Mice were maintained in individually ventilated cages and were fed a normal chow diet. Wild-type and SIRT6 heterozygous mice were obtained from Jackson Laboratory, USA. SIRT6 knockout mice were obtained by crossing the heterozygous mice. SIRT6 heterozygous male mice were harvested at the age of 3 months. Both males and females of SIRT6 knockout mice were sacrificed at 24-26 days of age. The heart tissues were collected and stored at −80°C after snap freezing in liquid nitrogen. These tissues were then used for whole-cell lysate preparation and total RNA isolation. For high-fat diet studies, 3 months old C57BL/6J wild-type male mice were fed a high-fat diet for a period of 12-15 weeks. The composition for the high-fat diet is available on request.

Human heart samples

All research related to human patients was reviewed and approved by the Institute's ethical committee. Both males and females were recruited to the study. The heart tissue samples were collected from patients during cardiac surgery by endomyocardial punch biopsy. Patients were identified based on the degree of heart failure, and patients having left heart failure with associated right ventricular failure and a TAPSE < 20 mm were enrolled. Informed consent was obtained from the patients. The mean age of human patients involved in the study is 44.39 ± 14.31 year (Mean ± s.d). Control samples were collected by biopsies from hearts which were donated for homograft banking, or from forensic autopsies of individuals without any known cardiovascular pathology. Samples were snap-frozen in liquid nitrogen and stored at −80°C. We are not sharing the complete details of the patients, as this work is a part of another study, which is being currently undergoing. The detailed patient information will be available upon request.

METHOD DETAILS

RNA Isolation and qPCR analysis

The cultured cells or the *in vivo* tissue samples were homogenized in the TRI-reagent (TAKARA). Total RNA was extracted using the manufacturer's protocol. 1 μg of total RNA was reverse transcribed using the iScript cDNA synthesis kit (BioRad), and qPCR was performed using the SYBR-Green PCR master mix in a real-time PCR system.

RNA-seq and ChIP-seq analysis

The detailed protocols for the RNA-seq and ChIP-seq experiments were described previously (Etchegaray et al., 2019). The analysis of fatty acid transporter gene expression was performed using data from our previous RNA-Seq dataset (Etchegaray et al., 2019), (GEO: GSE130690). SIRT6 binding peaks in the promoters of fatty acid transporter genes were analyzed using previous ChIP-Seq datasets available from hESC (GEO: GSE130689), K562 cells (ENCODE ID - ENCSR000AUB) and H1 cells (ENCODE ID - ENCSR000AUS). The ChIP-Seq datasets were analyzed as described in our previous work (Ravi et al., 2019). The co-ordinate file for the transcription start site was obtained from the UCSC table browser. The binding peaks were visualized using the Integrated Genome Viewer.

Preparation of cell lysates

The frozen *in vivo* tissues samples were crushed in liquid nitrogen and then homogenized and lysed in RIPA buffer (20 mM Tris–HCl pH 7.5, 150 mM NaCl, 1 mM EDTA, 1 mM EGTA, 1% NP-40, 1% sodium deoxycholate, 2.5 mM sodium pyrophosphate, 1 mM sodium orthovanadate, 5mM nicotinamide,1mM PMSF and 1X protease inhibitor cocktail). The lysates were then centrifuged at 12,000 rpm for 15 min at 4°C, and the supernatant was collected in a fresh tube. Cultured cells were harvested and lysed with ice-cold cell lysis buffer (20 mM Tris–HCl pH 7.5, 150 mM NaCl, 1 mM EDTA, 1 mM EGTA, 1% Triton, 2.5 mM sodium pyrophosphate, 1 mM sodium orthovanadate, 1 mM PMSF and 1X protease inhibitor cocktail) and the supernatant was collected following centrifugation.

Electrophoresis and immunoblotting

Bradford assay was performed to quantify protein lysates. Samples were normalized for an equal amount of protein. The lysates were then mixed with 2X Laemmli Sample Buffer with 5% β-mercaptoethanol and denatured by boiling at 95°C for 5 min. The samples were later electrophoresed on 12% or 15% SDS-PAGE gels and transferred onto 0.45 μm PVDF membranes by overnight wet transfer. 5% milk in TBST(Tris-buffered saline supplemented with 0.05% Tween 20) was used to block membrane for 1h at room temperature followed by overnight incubation at 4°C with specific primary antibody prepared in 5% BSA in TBST. A secondary antibody conjugated with horseradish peroxidase was incubated for 1 h at room temperature. The blots were washed thrice with TBST for three minutes each between each of the steps. ECL reagent was used to detect chemiluminescence, and the images were acquired using a chemiluminescence imager.

Immunoprecipitation assays

The cells were lysed in cell lysis buffer, and a specific antibody or normal rabbit IgG was added to 1mg of total protein. The samples were incubated overnight at 4°C with rotation at 5 rpm in a rotator. The antibody-bound protein complexes were then captured on protein A magnetic beads (BioRad Sure beads), which was then eluted in 2X Laemmli buffer and proteins analyzed by western blotting.

Fatty acid accumulation assay

Fatty acid accumulation assay was performed using BODIPY 493/503 (4,4-Difluoro-1,3,5,7,8-Pentamethyl-4-Bora-3a,4a-Diaza-s-Indacene) dissolved in Dimethyl Sulphoxide (DMSO) at the concentration of 2mg/ml. Cells were fixed, washed thrice with 1x PBS and stained with BODIPY (dilution of 1:300 in 1x PBS) for 30 minutes. The cells were then washed again with 1x PBS, and nuclear staining was done with Hoechst 33342. Finally, the cells were mounted on a clean glass cover slide using the Fluoromount-G Aqueous Mounting Medium and used for confocal microscopy.

Fatty acid uptake assay

Fatty acid uptake assay was performed using fatty acid analog BODIPY FLC12 (4,4-Difluoro-5,7-Dimethyl-4-Bora-3a,4a-Diaza-s-Indacene-3-Dodecanoic Acid). BODIPY was dissolved in dimethyl sulphoxide at a concentration of 1mg/ml. It was used in 1:500 dilution in serum-free DMEM. Cells were seeded in 24 well plates followed by transfection with appropriate plasmids/siRNA. Sixty hours post-transfection, cells were then treated with a BODIPY solution for 30 minutes. Cells were further washed thrice with PBS and used for flow cytometry or immunofluorescence microscopy.

Immunofluorescence microscopy

The cells were seeded on sterilized glass coverslips placed inside a 24-well plate. After necessary treatments, the cells were fixed using 3.7% formaldehyde for 15 min at room temperature and later permeabilized using 0.2% Triton X-100 for 5 min at room temperature. The cells were then blocked with 5% BSA in PBST for 1h and incubated overnight at 4°C with primary antibodies prepared in the 5% BSA in PBST (dilutions range1:50–1:200). The primary antibodies bound to the targets were detected by incubating cells with species-specific Alexa Fluor conjugated secondary antibodies prepared in 5% BSA in PBST for 1 h at room temperature. Nuclear staining of cells was carried out with Hoechst 33342 for 5 min at room temperature. The cells were washed twice with 1X PBS, between each step. Finally, the cells were mounted on a clean glass cover slide using the Mounting Medium, and the images were acquired using Zeiss LSM 880 confocal microscope in Airy scan mode.

Chromatin immunoprecipitation assay

The procedure for *in vivo* ChIP performed using the heart tissue sample was adapted from a previous study (Cotney and Noonan, 2015). Briefly, the tissue was homogenized, cross-linked using 1% formaldehyde for 15 min and quenched subsequently with 150 mM final concentration of glycine. The tissue was then harvested by centrifugation at 2000 g for 10 min at 4°C. Sonication was standardized with 25 s on and 40 s off for a total of 15 cycles. Sheared chromatin was then visualized on the agarose gel, which ranged in size from 200bp to 600bp. 50 μg of chromatin was then used for immunoprecipitation. For ChIP-re-ChIP analysis, SIRT6 bound chromatin fragments were immunoprecipitated from wild-type mice heart followed by elution at 50°C with ChIP elution buffer and vortexing at 700RPM for 30 minutes in. Eluted chromatin was further diluted with ChIP dilution buffer and used for PPARγ ChIP.

Histology analysis

The mice hearts were collected and frozen in optimal-cutting temperature solution (Invitrogen) for Oil Red O staining. Transverse frozen heart sections of 10μm were air-dried for 30 minutes and fixed in 10% formalin as described previously (Herman-Edelstein et al., 2014). Briefly, after dipping the slides in 60% isopropanol for 1 minute, they were stained in working Oil-Red-O solution (Sigma-Aldrich) for 15 minutes, followed by treatment with 60% isopropanol for 1 minute. After dipping in distilled water, the slides were counterstained with hematoxylin for 1 minute and then washed with distilled water again, followed by mounting with the aqueous medium. Digital images of sections were acquired using Olympus BX51 microscope with Pro rec C3 software.

Identification of putative binding residues on SIRT6 and PPARγ

Instead of performing blind docking with SIRT6 and PPARγ, we predicted likely interface residues on both the structures and used them as restraints while docking. To predict the putative interface residues, we performed multiple sequence alignment of SIRT6 and PPARγ with their respective homologs using CONSURF (Ashkenazy et al., 2016). Residues at the interfaces are partially conserved during evolution; hence, such partially conserved or conservatively substituted, solvent-exposed residue patch was identified for both structures. The following residues were used as restraints for docking:

SIRT6: R173, C175, R180, T182, I183, L184, D185, W186, E187, D188, L190, P191, D194, and D206; PPARγ: F121, H122, E129, K132, R136, R137, R159, N160, Q163, H177, and R184

Molecular docking for SIRT6 and PPARγ interaction

We performed a structure-based analysis to predict the binding mode of SIRT6 with PPARγ. Multiple structures for SIRT6 and PPARγ are available in the Protein Data Bank (PDB) (Berman et al., 2000). For SIRT6, we chose a structure (PDB code: 3pki) that was determined at a high resolution (2.0 Å) and had structural coverage for residues 11-295 with no missing residues in between (Pan et al., 2011). For PPARγ, the structure with PDB code 3e00 was chosen, which has a resolution of 3.1 Å and has structural coverage for both the DNA-binding and the ligand-binding domains (Chandra et al., 2008). But the structure is present in the complex with RXRα nuclear receptor (which makes the functional form of this heterodimeric nuclear receptor); hence, we considered the PPARγ chain for our analysis. Missing residues in the PPARγ structure were modeled using ModLoop (Fiser and Sali, 2003). The final structures (SIRT6 and PPARγ) were used as inputs for protein-protein docking using HADDOCK and HDOCK (van Zundert et al., 2016; Yan et al., 2017). We have supplied predicted interfacial residues to guide the protein-protein docking.

Identification of putative interface residues on SIRT6 and PPARγ

We identified homologs for SIRT6 and PPARγ using CONSURF webserver (Ashkenazy et al., 2016). Through CONSURF, we employed the homology detection tool, HMMER (Finn et al., 2011), for three iterations and e-value cut-off of 10^{-04}. 5527 unique homologs were identified for SIRT6 and 982 for PPARγ, out of which 150 sequences that represent the list of homologs to the queries were taken for multiple sequence alignment (MSA). MSA was performed by CONSURF using MAFFT (Katoh and Standley, 2014), algorithm. Partially conserved or conservatively substituted residues, which are also solvent-exposed (solvent accessibility $\geq$ 7%, calculated from NACCESS tool), were considered as putative interface residues. Since many residues could be identified, we ranked them based on (a) Continuum of residues forming a patch on the structure, (b) the Compatible residue properties between the two interfaces. For SIRT6, the following residues were ranked:

Rank 1: R173, C175, R180, T182, I183, L184, D185, W186, E187, D188, L190, P191, D194, and D206
Rank 2: K13, G14, G17, E20, D23, A51, G52, A56, V68, W69, R74, P78, F80, G103, Q111, and V113
For PPARγ, the following ranks were decided:
Rank1: F121, H122, E129, K132, R136, R137, R159, N160, Q163, H177, and R184
Rank 2: R140, L141, K142, L143, H155, K157, S158, K161, E189, and K190

Docking was first performed using HADDOCK, and HDOCK using rank 1 residues as restraints for interface residues and later using rank 2 residues as restraints (van Zundert et al., 2016; Yan et al., 2017). Since results for rank 2 patches were not promising according to the HADDOCK scores, we closely analyzed the results for rank 1 patches. Further, the HDOCK results for rank 1 residues did not satisfy the restraints, hence they are also not reported further.

Analysis of docking poses obtained from HADDOCK

HADDOCK is a well-known tool to predict protein-protein binding poses and provides multiple solutions, which are grouped into various clusters based on similarity in their binding. The top 2 clusters obtained from HADDOCK were taken forward for further analysis. The first cluster had 12 members and, the second cluster had 28 members. Though the lowest energy binding pose was a part of the top cluster, both the clusters had similar statistics in terms of HADDOCK score (−111.8 ± 110.1 and −111.1 ± 6.9 respectively) and z-score (−1.6 and −1.6 respectively). So, in practice, members from both the cluster could be taken as final solutions. Since we wanted to have one best possible solution; we further analyzed the binding poses of the top 4 members from both clusters manually. First, we checked for the number of restraints satisfied in the models. We used our in-house webserver, PIC, for this analysis, and the results are as follows (Tina et al., 2007). Putative interface residues provided as restraints for SIRT6 and PPARγ are given in the first and ninth column. The remaining columns show the best 4 models from the top 2 clusters. Y/N shows if restraint was satisfied in the model or not.

SIRT6 residues	5_1	5_2	5_3	5_4	2_1	2_2	2_3	2_4	PPARγ residues	5_1	5_2	5_3	5_4	2_1	2_2	2_3	2_4
173	Y	Y	N	Y	N	N	N	N	121	Y	Y	N	N	Y	N	N	N
175	N	N	N	N	N	N	N	N	122	Y	Y	Y	Y	Y	Y	Y	Y
180	Y	Y	Y	N	Y	Y	Y	Y	123	Y	Y	Y	Y	Y	Y	Y	Y
182	N	N	N	N	N	N	N	N	129	Y	Y	Y	N	Y	Y	Y	Y
183	N	N	N	N	N	N	N	N	132	Y	Y	Y	Y	Y	Y	Y	Y
184	N	N	N	N	N	N	N	N	136	Y	Y	Y	Y	Y	Y	Y	Y
185	Y	Y	Y	Y	Y	Y	N	Y	137	N	N	N	N	Y	Y	Y	Y
186	Y	Y	N	Y	N	N	N	N	159	N	N	N	N	Y	N	Y	N
187	Y	Y	Y	Y	Y	Y	Y	Y	160	N	N	N	N	Y	N	Y	N
188	Y	Y	Y	Y	Y	Y	Y	Y	163	N	N	N	N	N	N	N	Y
190	Y	Y	Y	Y	N	N	Y	Y	177	Y	Y	Y	Y	Y	N	N	N
191	N	N	N	N	N	N	N	N	184	Y	Y	Y	Y	N	N	N	N
194	N	N	N	N	N	N	N	N									
206	N	N	N	N	N	N	N	N									

From this analysis, we shortlisted model 5_1 and 2_1. Next, we calculated the interface area (using PDBePISA webservice) and interaction energy (using foldx tool)for both of the models (Schymkowitz et al., 2005). The interface area for 5_1 and 2_1 was found to be 840 Å^2 and 1050 Å^2. Both values are less than 1500 Å^2, a characteristic property of transient protein-protein interactions. The interaction energy was found to be comparable (−10.3 Kcal/mol and −13.0 Kcal/mol respectively for 5_1 and 2_1). Next, we compared the binding poses of 5_1 and 2_1 with the PPARγ-RXRα-DNA bound protein (PDB code: 3e00). Interestingly, 5_1 showed no steric clash with the RXRα chain and only overlapped with the DNA binding site suggesting that this binding pose should not disturb the biologically functional PPARγ-RXRα assembly. However, 2_1, on the other hand showed a steric clash with DNA as well as RXRα chain and might disrupt the PPARγ-RXRα assembly. Hence, 5_1 was selected as the final putative binding pose between SIRT6 and PPARγ.

Analysis for PPARγ binding sequence on CD36 promoter

To search for the presence of PPARγ binding sequences on the promoter of CD36 bound by SIRT6 as shown by ChIP Seq data analysis we used LASAGNA tool (Lee and Huang, 2013). The sequence of the binding sites thus obtained were compared with the sequence of CD36 and CAV1 promoter region on SIRT6-H1 ESCs ChIP Seq data retrieved from IGV. The details are presented in Table S2.

QUANTIFICATION AND STATISTICAL ANALYSIS

Graph-pad prism version 6.04 was used for statistical analysis and graph preparation. Student's t test was used for pairwise comparisons. For multiple comparisons, one-way and two-way ANOVA was used. Please note that statistical details are found in the figure legends. For confocal image analysis, ZEN-Black software was used, and ImageJ was used for quantification of western blots.